


RESEARCH ARTICLE

# Laboratory simulations of prebiotic ponds to investigate the impact of ultraviolet radiation on glycine dissolved in aqueous solutions

Alexandra Zetterlind<sup>1,\*</sup>, Nina Kopacz<sup>1,\*</sup>, Luise Jumpertz<sup>1</sup>, Salomé Lagasse De Loch<sup>1</sup>, Alexander Schneidt<sup>1</sup>, Sander Deelen<sup>2</sup>, Matthijs Krijnen<sup>2</sup>, Hugo van Ingen<sup>3</sup>, Eric Hellebrand<sup>1</sup> and Inge Loes ten Kate<sup>1</sup>

<sup>1</sup>Department of Earth Science, Utrecht University, Utrecht, Netherlands

<sup>2</sup>Instrumentatie, Utrecht University, Utrecht, Netherlands

<sup>3</sup>Bijvoet Centre for Biomolecular Research, Utrecht, Netherlands

**Corresponding authors:** Alexandra Zetterlind; Email: [a.o.zetterlind@uu.nl](mailto:a.o.zetterlind@uu.nl); Nina Kopacz; Email: [k.a.kopacz@gmail.com](mailto:k.a.kopacz@gmail.com)

**Received:** 22 February 2025; **Revised:** 08 May 2025; **Accepted:** 24 May 2025

**Keywords:** photochemistry; prebiotic chemistry; brines; ferrocyanide lakes; early Earth; early Mars; origin-of-life

## Abstract

For shallow ponds to be contenders for the venue of the emergence of life on Earth, they would have had to provide sufficient protection from ultraviolet (UV) radiation to allow for the preservation of organic molecules. Shallow ponds of a variety of compositions are proposed for early Earth, many of which may have provided ample shielding effects by attenuating UV light via absorption by (in)organic ions. Here, we present an experimental setup designed to simulate an irradiated water column to investigate the preservation/degradation of organic molecules and by proxy the attenuation of UV radiation in ponds of diverse compositions. In this setup, we dissolved glycine in ultrapure water, ferrocyanide and carbonate pond simulants and irradiated for several days. Our findings indicate that glycine's photochemical degradation under UV irradiation is minimal in the carbonate pond, though significant in the ferrocyanide pond and in ultrapure water, where it breaks down into diverse products including formamide, glycineamide, glycine methylester and acetaldehyde. Though ferrocyanide is a potent UV absorber, our experiments show ferrocyanide ponds to be transiently UV-shielding environments due to the removal of ferrocyanide by UV-induced precipitation of goethite and pyrite mineral assemblages and subsequent photodegradation of glycine in the cleared water column. Our results further suggest that hypersaline, carbonate ponds may present stable environments for prebiotic chemistry while providing ample UV attenuation, ultimately protecting the integrity of organic molecules. This work contributes to understanding the interplay between UV irradiation and (in)organic compounds in ponds and the suitability of those ponds for the onset of prebiotic chemistry on Earth, Mars and other celestial bodies.

## Contents

<b>Introduction</b>	<b>2</b>
UV-driven photochemistry of glycine	3
Photochemistry in ferrocyanide ponds	4
Photochemistry in carbonate ponds	4
<b>Methods</b>	<b>5</b>
Experimental setup	5
Sample preparation and experimental procedure	7

\*A.Z. and N.K. contributed equally to the work and this manuscript.

Analysis of organics in solution post-irradiation . . . . .	9
<i>Identifying photodegradation products in irradiated solutions of glycine in UPW</i> . . . . .	10
Analysis of UV-induced precipitation products . . . . .	10
<i>Infrared spectroscopy of ferrocyanide pond precipitate</i> . . . . .	10
<i>Microscopy and elemental analysis of ferrocyanide pond precipitate</i> . . . . .	10
<i>Elemental analysis of ferrocyanide pond solution post-precipitation</i> . . . . .	11
<b>Results</b> . . . . .	<b>11</b>
Precipitation induced by irradiation of pond analogues. . . . .	11
<i>Mineralogical composition of precipitate suggested by analysis of active vibrational modes</i> . . . . .	11
<i>Elemental composition and distribution of precipitates elucidated by SEM/EDS</i> . . . . .	12
<i>Concentrations of iron in ferrocyanide pond solution post-irradiation</i> . . . . .	12
UV irradiation of glycine . . . . .	13
<i>Glycine in ultrapure water</i> . . . . .	13
<i>Glycine in ferrocyanide ponds</i> . . . . .	14
<i>Glycine in carbonate ponds</i> . . . . .	14
<b>Discussion</b> . . . . .	<b>15</b>
Comparison of UV protection properties of ferrocyanide and carbonate prebiotic ponds . . . . .	15
<i>UV-induced precipitation and photochemistry in ferrocyanide ponds</i> . . . . .	15
<i>UV protection and resulting stability in carbonate ponds</i> . . . . .	19
Implications for astrobiology . . . . .	20
<i>Transient ferrocyanide ponds on Mars offer a window into prebiotic Earth</i> . . . . .	21
<i>Brines across the Solar System present a multitude of potential cradles for life</i> . . . . .	21
<b>Conclusion</b> . . . . .	<b>22</b>

## Introduction

Constraining the environmental conditions and geological settings of early Earth are among the fundamental questions addressed in origin-of-life studies. Several settings have been suggested as candidate environments from which life emerged (see Camprubí *et al.*, 2019, for an overview), one of which is the emergence of life on land. During the Hadean Eon, 4.6–4.0 Ga ago, warm, aqueous environments may have served as venues for the onset of prebiotic chemistry (e.g. Pace, 1991; Stetter, 2005). The first landforms to emerge from the global ocean during the Hadean were volcanoes, most likely consisting of subaerial hydrothermal fields with multiple hot springs, geysers and small pools (van Kranendonk, 2010; Bada and Korenaga, 2018; Djokic *et al.*, 2021) and meteorite craters that could also have served as depressions for ponds (Osinski *et al.*, 2020). These chemically distinct, potentially interconnected small bodies of water could have concentrated, diversified and complexified organic molecules within and between them (Santosh *et al.*, 2017; Damer and Deamer, 2020). This multiplex environment in effect served as a geochemical “laboratory” consisting of various types of aqueous solutions driving diverse sets of organic chemical reactions.

In this origin-of-life-on-land scenario, biochemical precursors would have been either endogenous or exogenous in origin. The frequent impact events during the Hadean delivered essential elements and organic molecules to early Earth’s surface (Bada and Korenaga, 2018), likely allowing for organic molecules to accumulate in early ponds. In addition to exogenous sources, there may have been endogenous synthesis of organics driven by shock synthesis from impacts, energy from UV light, electrical discharges or geological electrochemical energy (Chyba and Sagan, 1992; Deamer and Weber, 2010).

Standard solar models predict that the Sun’s luminosity in the early days (before 3.8 Ga) was 70–77% of its present brightness (Gough, 1981; Bahcall *et al.*, 2001), so the surface solar heating was less intense than today. The luminosity in the UV part of the spectrum, however, was likely much higher in the past (Cnossen *et al.*, 2007), and the lack of atmospheric O<sub>3</sub> allowed the full range of UV between 200 and 400 nm to reach the surface (Claire *et al.*, 2012; Cockell, 2000). The big challenge for prebiotic

chemistry on early Earth's surface was, hence, the harsh UV environment. Though UV-dependent reactions are thought to have been crucial in prebiotic chemistry, full exposure of chemical systems to UV radiation would likely have been too destructive to organic molecules for complex systems to emerge.

Prebiotic organic compounds may have been protected by atmospheric absorbers such as gaseous hydrocarbons and organic hazes within primordial transient reducing atmospheres (Yoshida *et al.*, 2024). This scenario is analogous to early Earth's natural waters, where organic molecules and dissolved ions may have served as "sunscreen" molecules in the aqueous solutions of shallow prebiotic ponds, thus enhancing the preservation of organic molecules over time and water depth (Ranjan *et al.*, 2022; Todd *et al.*, 2022, 2024). The UV transmission of prebiotic natural waters has been investigated, revealing that different water types exhibit varying levels of UV shielding. Prebiotic freshwater ponds were found to be predominantly transparent to UV radiation. Ferrocyanide lakes demonstrated strong attenuation of UV radiation, while saline, carbonate lakes were characterized by limited short-wave UV flux attenuation (Ranjan *et al.*, 2022).

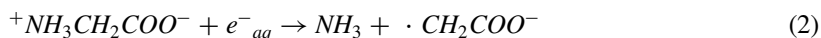
To investigate the survivability of prebiotically relevant organic molecules in early terrestrial ponds, we designed a wet chemistry setup to simulate a stagnant, irradiated water column. We investigated the fate of the amino acid glycine (NHCH<sub>2</sub>COOH) dissolved in ultrapure water, a ferrocyanide pond analogue and a carbonate pond analogue subjected to UV irradiation, both over time and depth. We used glycine as it is the simplest of the amino acids and has been studied broadly as a model organic molecule (ten Kate *et al.*, 2005, 2006; Garry *et al.*, 2006). Glycine absorbs UV radiation below 220 nm (see Fig. 7; ten Kate *et al.*, 2005) and makes up a large fraction of the amino acid content of carbonaceous chondrite meteorites (Cobb and Pudritz, 2014; Sephton, 2014; Glavin *et al.*, 2018). Experiments have shown that glycine effectively leaches out from aqueously submerged meteorites within days, making a strong argument for the presence of ponds enriched in glycine on early Earth (Zetterlind *et al.*, 2024).

### UV-driven photochemistry of glycine

Glycine degrades under the influence of UV light and photodissociates into smaller molecules such as ammonia (NH<sub>3</sub>), amines, CH<sub>2</sub>NH<sub>2</sub> and CO<sub>2</sub>H, carbon dioxide (CO<sub>2</sub>) and various free radicals (Gerakines *et al.*, 2012; Lee and Kang, 2015). Throughout this process, photons break glycine's molecular bonds and gradually remove its functional groups. Irradiated glycine can undergo two primary destruction mechanisms: decarboxylation and deamination. In the decarboxylation reaction, glycine gets oxidized through one-electron transfer, followed by the transfer of a proton (H<sup>+</sup>) and finally by the removal of a hydrogen atom from a neighbouring molecule, resulting in the formation of an amine and a CO<sub>2</sub> molecule (Gerakines *et al.*, 2012):



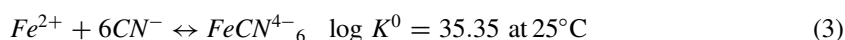
The expected amine product for glycine is methylamine (NH<sub>2</sub>CH<sub>3</sub>) (Gerakines *et al.*, 2012). Deamination of glycine yields ammonia and a free radical:



The radical can extract a hydrogen atom to form a carboxylic acid (Gerakines *et al.*, 2012). The deamination and decarboxylation products can undergo further photodegradation, resulting in the formation of smaller chemical groups, with CO<sub>2</sub> being the dominant photoproduct (Ehrenfreund *et al.*, 2001). In addition, UV radiation can also affect surrounding atmospheric oxygen and water molecules, generating reactive oxygen species including H<sub>2</sub>O<sub>2</sub>, OH<sup>-</sup>, HO<sub>2</sub> and solvated electrons e<sup>-</sup><sub>aq</sub>. These species can further participate in the degradation of glycine (Oró and Holzer, 1979; de Jager *et al.*, 2017).

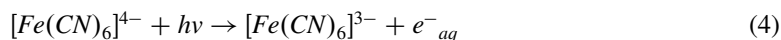
### Photochemistry in ferrocyanide ponds

We investigated ferrocyanide ponds since cyanide plays an important role in the organic synthesis of many molecular building blocks of life. The reductive homologation of hydrogen cyanide (HCN) can form precursors of ribonucleotides, amino acids and lipids (Xu *et al.*, 2018). UV light, copper, sulphur and phosphorus can be drivers for these productions (Patel *et al.*, 2015; Toner and Catling, 2019). Cyanide may have been present on early Earth due to HCN production from photochemistry and subsequent photolysis (Zahnle, 1986; Tian *et al.*, 2011) and from delivery by meteoritic infall and atmospheric processing (Sasselov *et al.*, 2020). However, significant concentrations of HCN are needed for prebiotic cyanide chemistry, which would have required a CH<sub>4</sub> inventory that is unrealistic in steady-state on the early Earth (Pearce *et al.*, 2022). Rather, HCN was probably only transiently present in the aftermath of large impacts (Wogan *et al.*, 2023; Zahnle *et al.*, 2020). Iron ions on early Earth's surface could have reacted with cyanide to form aqueous ferrocyanides and provide a natural concentration mechanism (Watt *et al.*, 1965; Toner and Catling, 2019):

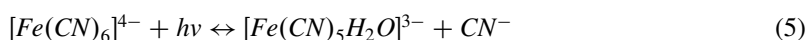


Measured and computed absorption of UV-active components in simulated ferrocyanide ponds indicates a strong UV absorbance through ferrocyanide (Ranjan *et al.*, 2022). These calculations suggest that while ferrocyanide is expected to exhibit the highest UV absorption, other ions such as sulphite (SO<sub>3</sub><sup>2-</sup>), bisulphite (HSO<sub>3</sub><sup>-</sup>) and nitrate (NO<sub>3</sub><sup>-</sup>) are also predicted to significantly contribute to UV absorption across a broad spectral range. Sulphite serves as both a UV-absorbing species and a component in a UV-driven photoredox cycle when paired with ferrocyanide (Todd *et al.*, 2022).

UV photons in the 200–300 nm wavelength range facilitate the photooxidation of ferrocyanide, resulting in the generation of solvated electrons. These electrons can participate in chemical reduction processes relevant to prebiotic synthesis:



UV photons with wavelengths exceeding 300 nm induce the substitution of a cyanide ligand with a water molecule upon irradiation. This process, known as the reversible photoaquation of ferrocyanide, produces pentacyanoaquaferate and releases free cyanide:



If the reaction is not reversed, cyanide is effectively removed from the solution. The stability of ferrocyanide under irradiation can range from a few minutes to several hours or more, depending on factors such as pH, temperature and concentration (Todd *et al.*, 2022).

### Photochemistry in carbonate ponds

The second pond analogues we investigated were carbonate ponds, because of their ability to preserve phosphorus in a bioavailable form. Phosphorus is a critical element in essential biomolecules such as ATP, RNA, DNA and membrane phospholipids, playing a vital role in key biochemical processes (Westheimer, 1987; Schwartz, 2006; Fernández-García *et al.*, 2017). However, naturally occurring phosphate-rich waters are rare, as phosphate readily precipitates with calcium, forming apatite minerals (Ca<sub>5</sub>(PO<sub>4</sub>)<sub>3</sub>X) with low solubility (Maciá, 2005; Toner and Catling, 2020). This scarcity, referred to as “the phosphate problem,” presents a significant challenge to the evolution of biochemistry. One promising approach to addressing this issue involves investigating closed-basin carbonate ponds, where elevated carbonate concentrations promote the sequestration of calcium as calcium carbonate (CaCO<sub>3</sub>). This process minimizes the availability of calcium ions for apatite mineral formation, thereby preserving phosphate in more bioavailable forms (Toner and Catling, 2020). The geochemical composition of carbonate ponds facilitates the efficient weathering of apatite minerals, which subsequently enhances

condensation reactions such as phosphorylation and, more broadly, polymerization processes (Fox & Harada, 1958; Lahav *et al.*, 1978; Deamer & Weber, 2010). The boron present in carbonate ponds plays a critical role in promoting regioselectivity and stabilizing key reactions, including the phosphorylation of sugars and the synthesis of nucleic acids (Ricardo *et al.*, 2004). Moreover, these environments can accumulate cyanide compounds and sulphite ions, which as described above, can promote prebiotic chemistry both by shielding molecules from UV and by contributing electrons through a photoredox cycle (Toner and Catling, 2019).

Closed-basin carbonate lakes, in addition to supplying substantial quantities of phosphate and salts, may also offer environments conducive to shielding against UV radiation due to their elevated salt concentrations. Computational analyses of these saline waters indicate strong attenuation of shortwave ( $\leq 240$  nm) UV radiation (Ranjan *et al.*, 2022). This attenuation is primarily attributed to halide anions such as  $\text{Br}^-$  and  $\text{Cl}^-$ , which act as significant UV absorbers. Importantly, the absorption is dominated by anions, as cations do not exhibit absorption in the investigated spectral range (Birkmann *et al.*, 2018). The exposure to UV irradiation can induce photoelectron detachment from aqueous anions, including halides ( $\text{Cl}^-$ ,  $\text{Br}^-$  and  $\text{I}^-$ ) as well as sulphite and sulphide ions, leading to the formation of solvated electrons ( $e^-_{aq}$ ) and oxidized radicals. These species are highly reactive and can serve as initiators for subsequent chemical reactions (Jortner, 1964; Sauer *et al.*, 2004).

Studies utilizing ionizing radiation (gamma rays) have demonstrated that the presence of NaCl mitigates the damage to glycine. Irradiation of water leads to the formation of hydroxyl radicals (Melton and Neece, 1971) that in aqueous solutions attack glycine molecules. In saline solutions, however, the chlorine ions react with the hydroxyl radicals before they can attack the glycine, thus preserving the integrity of the glycine molecules (Cruz-Cruz *et al.*, 2020).

## Methods

We conducted a series of experiments to examine the effects of UV radiation on glycine in ultrapure water (UPW) and in simulated environments mimicking ferrocyanide and saline, carbonate ponds as described by Ranjan *et al.* (2022) and Rossetto *et al.* (2022). Glycine (Sigma-Aldrich,  $\geq 99\%$  HPLC grade), was used as a model organic molecule, as reported in prior studies (ten Kate *et al.*, 2005; Garry *et al.*, 2006; Johnson *et al.*, 2012; Lee and Kang, 2015; Poch *et al.*, 2013). A concentration of 25 mM was selected, representing a high-end estimate for glycine concentrations in prebiotic environments on early Earth (Lahav *et al.*, 1978; Fox *et al.*, 2019).

## Experimental setup

To replicate the conditions of a prebiotic pond water column, we built a modular, multicompartment tower featuring UV-opaque containers separated by UV-transparent windows, allowing us to pass a focused UV beam through the water column and sample it at different depths.

The modular tower consists of borosilicate glass containers with GL80 size threads, fit together with aluminium-threaded rings (Figure 1). As borosilicate plain GL80 screw thread wasn't available, we instead used 500 mL GL80 flasks and cut the screw thread from them. The glass containers were built using two GL80 screw threads and welded together with a piece of 85 mm (outer diameter) glass tube. The bottom aluminium cap forms the base of the tower and is protected from the UV beam by a polytetrafluoroethylene (PTFE-Teflon) sheet liner. The aluminium threads connecting the containers contain a fused silica (Suprasil) window at their centre, secured by a stainless-steel screw ring, a Teflon gasket and a fluoroelastomer (FKM-Viton) O-ring. The top aluminium cap has a Suprasil window for the UV beam to enter the tower unimpeded. The borosilicate glass that makes up the containers is UV-opaque to wavelengths shorter than 300 nm, while the Suprasil windows separating the containers are UV-transparent in the 200–400 nm range. Teflon and Viton materials are both highly resistant to

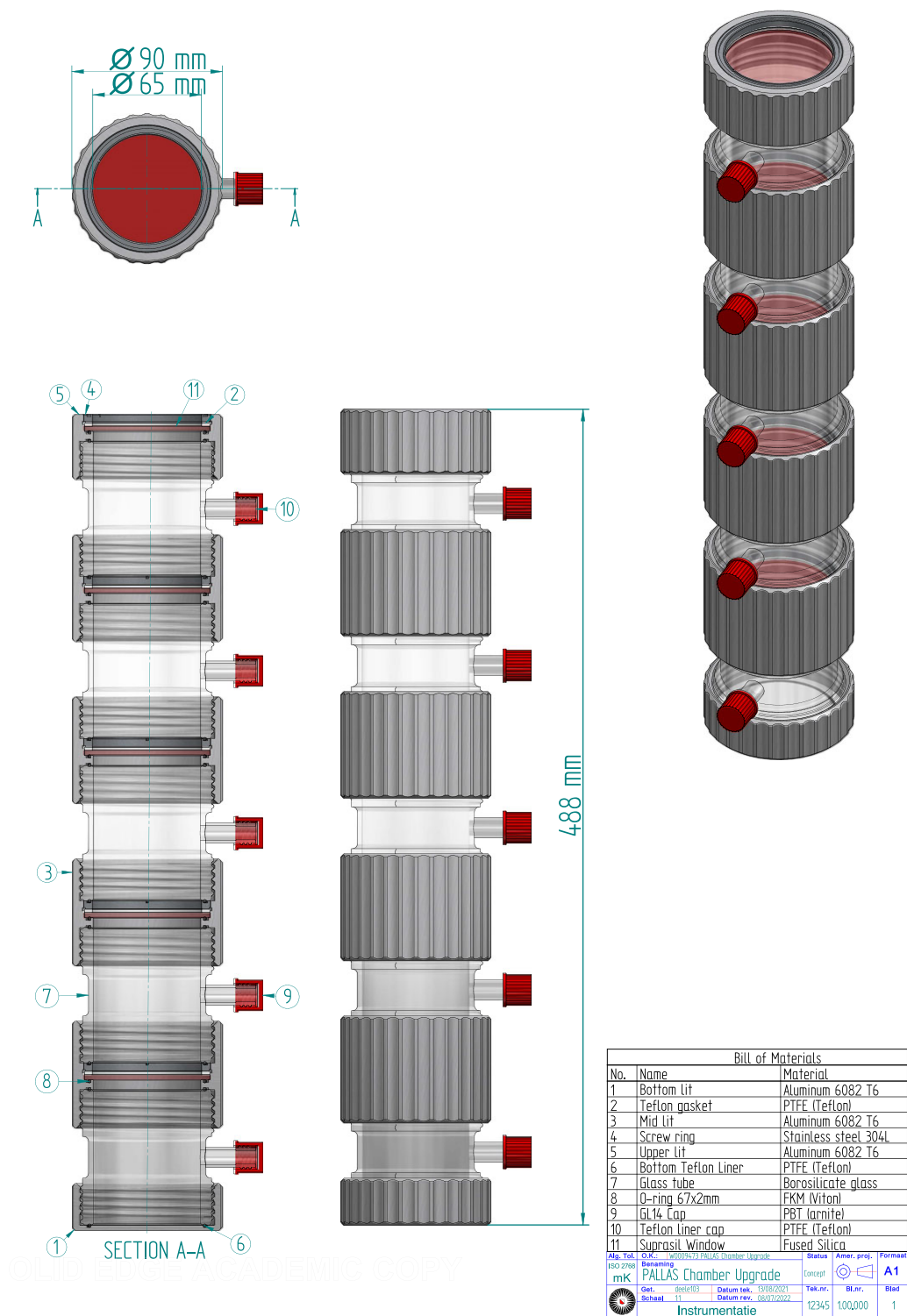


**Figure 1.** Schematic of modular, multi-compartment tower. The UV-opaque borosilicate glass containers are fit together with aluminium threaded rings and separated by UV-transparent Suprasil windows. The parts are labelled with numbers, and their corresponding specifications are listed in the table. The dimensions are shown in green.



chemical alteration and UV radiation and are thus neither expected to degrade nor produce contaminants.

Each container, with an approximate volume of 330 mL, is sealed with a Viton O-ring to prevent leakage and has a GL14 spout secured with a polypropylene cap with a Teflon insert. This allows for isolated sampling of each container throughout the experiment. For this experiment, we used five containers for the irradiated tower, referred to as C1–C5. C1 sits on top, simulating a depth of 30–40 cm below the pond surface, and C5 sits on the bottom, simulating a depth of 70–80 cm below the pond surface. A single-container tower is used as a dark control, referred to as CD. Both towers are placed in a 50 × 50 × 50 cm Planetary Analogues Laboratory for Light, Atmosphere and Surface Simulations (PALLAS) vacuum chamber with UV source and gas inlet (Figure 2) (ten Kate and Reuver, 2016). The C1–C5 tower is placed on a socle under the UV source, with C1 closest to the UV source. The CD tower rests on the dark side of the chamber, shielded from the UV beam by a metal construct. A gas inlet into the PALLAS chamber allows for nitrogen purging, removing any ozone that may be produced by the UV lamp. A 450 W Xenon arc lamp, with an output of  $5.42 \times 10^{18}$  photons s<sup>-1</sup> cm<sup>-2</sup> in the 200–400 nm spectral range (Fornaro *et al.*, 2018), is housed above the chamber. Its output is directed through a 30 cm-long borosilicate tube with Suprasil windows on the top and bottom, which is filled with water and serves as a heat sink, before entering the chamber through a Suprasil window and being directed into the tower. The UV output below 300 nm is thus entirely contained within the extended water column (including both the heat sink and the tower).

### ***Sample preparation and experimental procedure***

Before proceeding with any experimental steps, all materials used were thoroughly cleaned. Glassware was soaked in a 1% solution of Decon 90 in water for 24 hours. Metal and rubber parts were brushed with soap under running ultrapure (Milli-Q) water (UPW), and all parts were subsequently rinsed with UPW before being dried in an oven at 60°C. After drying, the parts were rinsed in a bath of methanol (PESTINORM, 99.7%) and then in a bath of hexane (PESTINORM, 99.7%) before being left to evaporate overnight under a chemical hood. They were then wrapped in aluminium foil and given a final rinse with UPW prior to use. When mineral salts were involved in the experiments, the materials were soaked in a 0.1 M HCl bath for a minimum of 6 hours before proceeding with the above-described cleaning procedure. These cleaning steps were taken to ensure that the materials were free of any contaminants that could potentially affect the results of the experiments.

To achieve anoxic conditions, oxygen was removed from the UPW by bubbling nitrogen gas through it overnight before adding the compounds (glycine and/or mineral salts) and mixing until fully dissolved. We performed tests prior to the experiments wherein we measured the oxygen levels in the water to determine the length of bubbling time needed and to ensure that the oxygen levels did not rise during the rest of the sample preparation procedure. Salts were purchased of the highest purity available from Merck, Sigma-Aldrich, Arcos Organics and Roth (see Tables 2 and 3). Each tower container was then filled with the solution, sampled with a Pasteur pipette (rinsed 3 times with UPW prior) and topped off to eliminate any air bubbles. Every 24 hours, the towers were taken out of the chamber and sampled under a chemical hood using a rinsed Pasteur pipette. To prevent oxygen diffusion into the solutions, the containers were flushed with argon gas while sampling to fill the headspace created in the containers by the removal of material. The time it took to sample was about 20 seconds, and no oxygen was measured to diffuse into the solutions at this time. Before starting the experiment, the chamber was cleaned with isopropanol, closed and flushed with nitrogen gas. The lamp was turned on and allowed to heat up for 15 minutes. The CD tower was then placed on the dark side of the chamber behind a metal barrier, and the C1–C5 tower was placed on a socle under the UV beam.

Three experiments were conducted to assess the survivability of glycine in simulated ponds. We investigated how glycine and various UV-active ions behave independently and combined under the

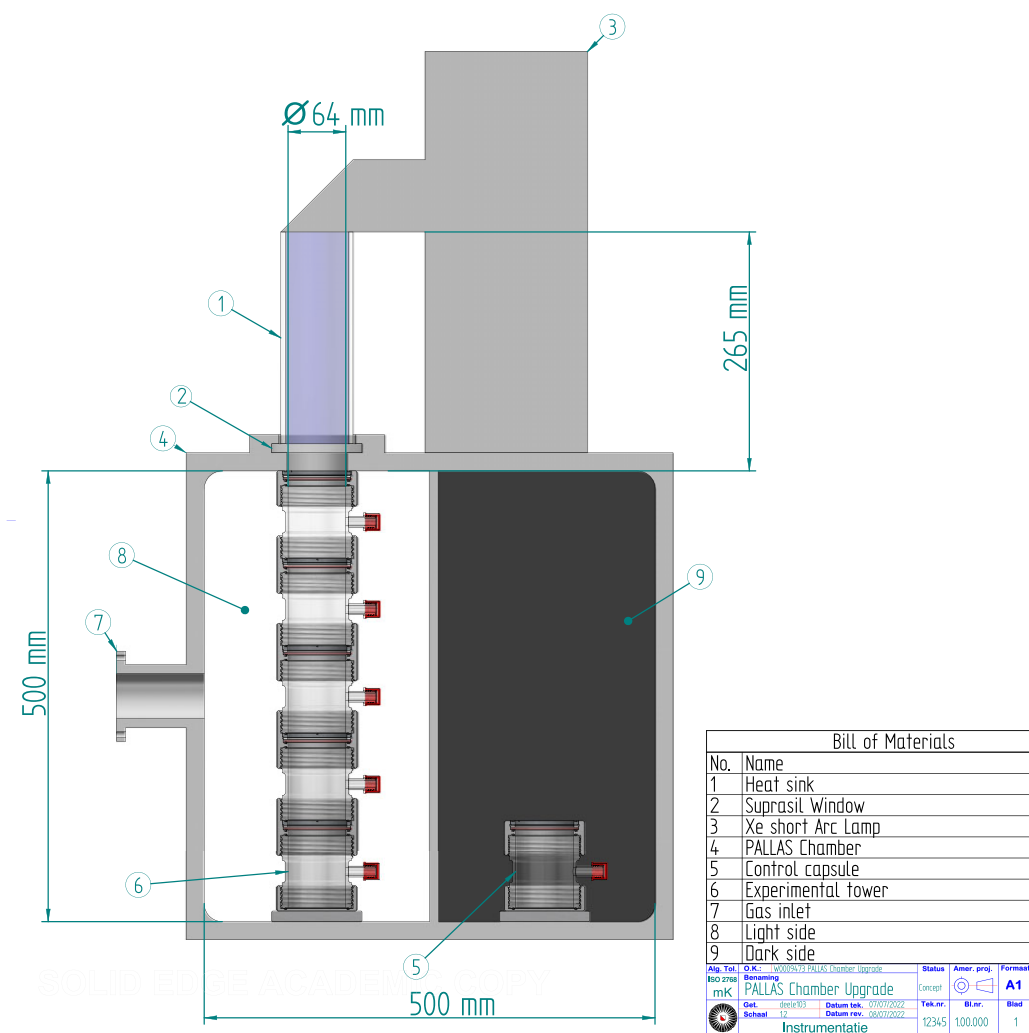


**Figure 2.** Schematic of PALLAS chamber including the water column tower setup. The UV beam passes through the 30 cm-long heat sink water column before entering the tower, allowing us to simulate five different depths between 30 and 80 cm below the stagnant pond surface. The parts are numbered and described in the table. The dimensions are shown in green.

influence of UV irradiation. For the first experiment (*glycine in UPW*, see Table 1), 25 mM of glycine was dissolved in anoxic UPW and irradiated for 6 days to measure the effect of UV irradiation on glycine without the added influence of ions. For the second experiment (*ferrocyanide pond + glycine*, see Table 1), 25 mM of glycine was added to the ferrocyanide pond solution shown in Table 2 and irradiated for 14 days. In the third experiment (*carbonate pond + glycine*, see Table 1), 25 mM of glycine was added to the carbonate pond solution shown in Table 3 and irradiated for 14 days. To achieve a clear and fully dissolved solution, it was necessary to omit calcium carbonate ( $\text{CaCO}_3$ ) and calcium chloride ( $\text{CaCl}_2$ ).  $\text{CaCO}_3$ , originally suggested by Ranjan *et al.* (2022) and present in the simulation of Rossetto *et al.* (2022), was excluded due to its limited solubility. The recipes of both ferrocyanide and carbonate solutions were purposely designed to maintain a near-neutral pH in order to keep glycine in its zwitterionic state. Carbonate lakes may have had a  $\text{pH} \gg 7$  (Toner and Catling, 2020), in which glycine could have been



**Table 1.** Overview of conducted experiments. Three experiments were conducted to investigate how glycine ( $\text{NH}_2\text{CH}_2\text{COOH}$ ) and UV-active ions behave independently and combined under the influence of UV irradiation.

Experiment	Solution (in UPW)	Figures
Glycine in UPW	25 mM glycine	8A
Ferrocyanide pond + glycine	See Table 2 + 25 mM glycine	8B
Carbonate pond + glycine	See Table 3 + 25 mM glycine	8C

**Table 2.** Ferrocyanide pond compositions, adapted from Ranjan et al. (2022) and Rossetto et al. (2022). All components were dissolved in anoxic UPW at a pH of 7.75.

Salt	Concentration	Purity
$\text{K}_4\text{Fe}(\text{CN})_6 \times \text{H}_2\text{O}$	0.10 mM	98.5–102.0%
NaBr	0.15 mM	99.0–100.5%
NaCl	0.20 mM	$\geq 99.0\%$
KI	600 nM	$\geq 99.5\%$
$\text{NaNO}_3$	0.010 mM	$\geq 99.5\%$
$\text{Na}_2\text{SO}_3$	0.10 mM	$\geq 98.0\%$
$\text{NaHSO}_3$	0.20 mM	$\geq 98.0\%$
$\text{Na}_2\text{SO}_4$	0.021 mM	$\geq 99.0\%$
$\text{Na}_2\text{CO}_3$	1.0 mM	$\geq 99.0\%$
$\text{MgCl}_2$	0.19 mM	$\geq 99.0\%$

**Table 3.** Carbonate pond compositions, adapted from Ranjan et al. (2022) and Rossetto et al. (2022). All components were dissolved in anoxic UPW at a pH of 7.75.

Salt	Concentration	Purity
NaCl	3.0 M	$\geq 99.0\%$
$\text{NaHCO}_3$	0.10 M	$\geq 99.0\%$
$\text{Na}_2\text{HPO}_4$	0.10 M	$\geq 98.0\%$
$\text{Na}_2\text{SO}_4$	0.10 M	$\geq 99.0\%$
$\text{H}_3\text{BO}_3$	0.10 M	$\geq 99.8\%$
KBr	10 mM	$\geq 99.0\%$
$\text{Na}_2\text{CO}_3$	7.0 mM	$\geq 99.9\%$
$\text{NaNO}_3$	1.0 mM	$\geq 99.5\%$
KI	600 nM	$\geq 99.5\%$
$\text{Na}_2\text{SO}_3$	0.40 mM	$\geq 98.0\%$

in its anionic state. In these experiments, we chose to keep glycine in its neutral state to simplify the experiment. Further investigations should involve exploring the pH gradients in simulated ponds.

#### *Analysis of organics in solution post-irradiation*

To obtain both qualitative and quantitative data, we prepared nuclear magnetic resonance (NMR) samples. The samples and the experimental blanks were composed of 440  $\mu\text{L}$  of a 25 mM solution of the

desired analyte, 100  $\mu\text{L}$  of internal standard potassium hydrogen phthalate (KHP, starting concentration of 25 mM) and 60  $\mu\text{L}$  deuterated water ( $\text{D}_2\text{O}$ ), respectively.

The analyses were conducted on a 600 Bruker NMR instrument equipped with SampleJet and Prodigy cold probe. Standard  $^1\text{H}$  1D spectra with excitation sculpting water suppression were recorded (zgesgp pulse sequence), with an acquisition time of 2.7 seconds, a recycle delay of 4 seconds and 256 scans (taking 30 minutes per 1D measurement). Prior to Fourier Transform using Bruker Topspin, spectra were processed using exponential line broadening of 0.3 Hz. The obtained spectra were analysed with Bruker TopSpin 4.2.0 and MestReNova (version 14.3.3-33362). Quantitative analyses were determined to be inadequate using this method and will therefore not be discussed further.

#### *Identifying photodegradation products in irradiated solutions of glycine in UPW*

Spiking tests were performed to confirm the possible photodegradation products using standards of compounds commonly suggested as photolysis products of glycine. Samples of irradiated solutions of 25 mM glycine in UPW were spiked with 200  $\mu\text{L}$  of distinct 25 mM solutions of glycineamide hydrochloride (98%), formamide ( $\geq 99.5\%$ ), acetaldehyde (99.5%), formaldehyde (99%), formic acid (99–100%), ethanol (96%), methanol (99%), ammonia (25%) and glycine methyl ester hydrochloride (99%) (all Merck Life Sciences N.V.). Additionally, reference spectra were obtained for each of these molecules. The comparison between reference spectra of known compounds with the obtained spectra of the photolysed samples coupled with a measurable effect from the spike tests allowed us to identify newly formed photodegradation products.

#### *Analysis of UV-induced precipitation products*

Upon irradiation in the tower, the solution in the *ferrocyanide pond* + *glycine* experiment turned yellow, and a precipitate formed in each of the C1–C5 containers. We thus repeated the experiment for an irradiation period of 11 days with solely the ferrocyanide pond solution without the addition of glycine (referred to as the *Fe salts-only* experiment) to study the interaction between UV radiation and the inorganic ions in the solution. The precipitates obtained from the *Fe salts-only* solution were dried down, first with a vacuum pump, then for 1 hour at  $30^\circ\text{C}$  in the oven and subsequently for two days in a freeze dryer. The elemental composition and mineralogy were analysed with infrared and X-ray spectroscopy and electron microscopy.

#### *Infrared spectroscopy of ferrocyanide pond precipitate*

The dried precipitate powder was ground with a pestle and mortar together with potassium bromide (KBr) powder in a ratio of 1:10 and analysed with a Nicolet 6700 IR Spectrometer from Thermo Fischer Scientific. A diffuse reflectance infrared Fourier transform (DRIFT) accessory was used, and infrared (IR) spectra were obtained with 64 scans per acquisition at a resolution of  $0.2\text{ cm}$  over a range of  $4000\text{--}400\text{ cm}^{-1}$ . A reference spectrum of in-house goethite (Fe(III) oxide-hydroxide) standard mixed with KBr in a ratio of 1:100 was obtained with the same method. The spectra of the precipitate samples from containers C1–C5 were compared to each other, to the reference spectrum of goethite and to the reference attenuated total reflectance (ATR) spectrum of pyrite (RRUFF ID: R050070.1) from the RRUFF database (Lafuente *et al.*, 2016).

#### *Microscopy and elemental analysis of ferrocyanide pond precipitate*

Secondary electron (SE) and backscattered electron (BSE) images of the precipitates in C1, C2, C3 and C5 were obtained using a Zeiss EVO 15 Scanning Electron Microscope (SEM) with a 10 mm working distance and the following beam conditions: C1: 15.00 kV, 150 pA; C2: 20.00 kV, 500 pA; C3: 20.00 kV, 500 pA; C5: 20.00 kV, 150 pA. The SEM was coupled with a Bruker XFlash 6160 energy-dispersive

X-ray (EDS) detector to characterize the elemental composition of the powder. C4 was excluded from SEM/EDS analysis due to previous changes in physical and chemical properties in the oven.

#### *Elemental analysis of ferrocyanide pond solution post-precipitation*

We used inductively coupled plasma optical emission spectrometry (ICP-OES) to measure the iron concentration left in solution in C1-CD of the Fe salts-only experiment (after 11 days of irradiation) and in C1-CD of the *ferrocyanide pond* + *glycine* experiment (after 14 days of irradiation). A 5 mL aliquot of each solution was measured on an AVIO500 ICP-OES (Perkin Elmer), equipped with a conical spray chamber, a micro-concentric Teflon nebulizer and a PrepFAST autosampler (SC-4 DX), with a sample flow rate of 300  $\mu\text{L}/\text{min}$ . Argon was used to generate the plasma (emission source). The pH of the solutions was measured with a pH electrode (Mettler Toledo, Seven compact Duo InLab 731-ISM).

## Results

### *Precipitation induced by irradiation of pond analogues*

No obvious visible changes were observed in the ultrapure water solutions (*glycine in UPW*) after irradiation. The potential decomposition of water into H and OH radicals cannot be measured in our setup. Similarly, no visible changes to the carbonate solutions (*carbonate pond* + *glycine*) were observed during or after the conclusion of the experiment. The pH in these solutions remained near neutral ( $7.33 \pm 0.05$ ) throughout the experiments.

Upon exposure to irradiation within the tower, the ionic ferrocyanide solutions (in both the *ferrocyanide pond* + *glycine* and the *Fe salts-only* experiment) exhibited a yellow colouration and generated a solid precipitate, though the amount of the precipitate was greater in the *Fe salts-only* experiment. The precipitate from the additional *Fe salts-only* experiment is shown in Figure 3. The yellow colour appeared after 24 hours in C1 and migrated towards the lower containers in the following days. After the solutions in the individual containers turned yellow, a yellow-orange solid precipitated out and the solution in the containers turned transparent once more (Figure 3A, B). No precipitate was formed in the dark control (CD). After irradiation for 11 days, C1 held the most precipitate, and the amount of precipitate decreased with increasing depth (Figure 3C). A detailed log of the onset of colouring and precipitate formation can be seen in Table S1. The pH of the ferrocyanide solutions (in both experiments) increased up to  $9.24 \pm 0.05$  post-irradiation.

### *Mineralogical composition of precipitate suggested by analysis of active vibrational modes*

The precipitate obtained from all five containers from the *Fe salts-only* experiment was dried and analysed with DRIFT spectroscopy. The precipitate spectra are compared to the reference spectra of pyrite and goethite (Figure 4). Pointed out with stars are the prominent peaks in the reference spectra of the minerals goethite and pyrite. A summary of the identified active bands and the corresponding vibrational modes can be found in Table 4. The yellow and orange arrows point out the peaks in our precipitates' spectra that may correspond to the peaks of pyrite (yellow) or goethite (orange). Containers C1, C2, C4 and C5 had a dip in their spectra around the placement of the IR active bands between 1049 and 974  $\text{cm}^{-1}$  (pointed out with the orange and yellow dotted arrow) that corresponds either to the S-S stretching modes of pyrite (Han *et al.*, 2020) and/or to specifically adsorbed sulphate groups on goethite (not seen in the reference spectrum of goethite since they are not part of the normal active bands of the mineral) (Gotić and Musić, 2007). The two very dominant IR bands at 895 and 799  $\text{cm}^{-1}$  are attributed to Fe-O-H bending vibrations that are very typical of goethite (shown with orange stars in the spectrum of goethite and suggested with orange arrows for the spectra of C1 and C2). A smaller band at 624  $\text{cm}^{-1}$  in the spectrum of goethite is assigned to Fe-O stretching vibrations, also characteristic of goethite structures (Verdonck *et al.*, 1982; Cambier, 1986; Gotić and Musić, 2007), though it is not prominent in

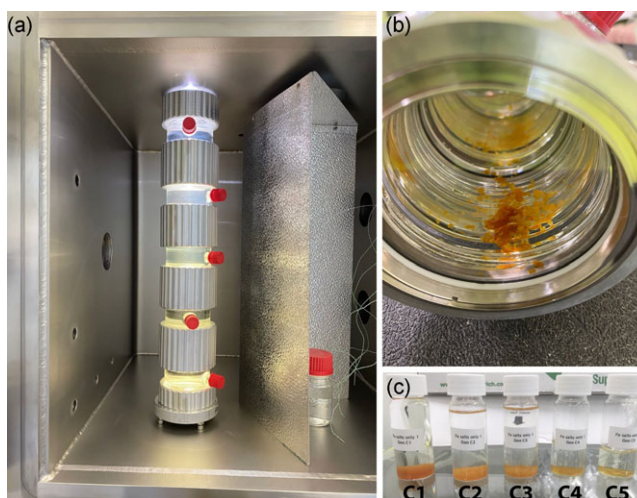


**Figure 3.** UV-induced precipitation in tower containing only the ferrocyanide pond solution. (A) The solution turned yellow upon irradiation, then clear once more after a solid precipitated out, first in C1 and subsequently in the lower containers. (B) The solid precipitate had a yellow-orange colour. (C) The recovered precipitate was most abundant in C1 and least in C5 after 11 days of irradiation.

any of our precipitate spectra. A very sharp peak can be seen in all of the spectra of C1–C5 around  $429\text{ cm}^{-1}$  (pointed out with the yellow arrow), which could correspond to the Fe–S<sub>2</sub> stretching mode of pyrite at  $420\text{ cm}^{-1}$  (marked by a yellow star) (Zheng *et al.*, 2019) though it is shifted in our case since the reference spectrum of pyrite used here was acquired with ATR instead of DRIFT).

#### *Elemental composition and distribution of precipitates elucidated by SEM/EDS*

The precipitates obtained from containers C1, C2, C3 and C5 from the *Fe salts-only* experiment were analysed with SEM/EDS. (C4 was excluded from analysis since it was altered in the drying procedure.) The precipitate from C1 appeared as fine-grained material under the microscope, with no discernible crystal structure (Figure 5A), as did the material from C2 and C3 (Figs. S1A, S2A). The precipitate from C5 showed more crystallinity (Figure 6A). All precipitate samples were found to contain iron, oxygen and sulphur (Figures 5B, 6B, S1B and S2B). The distribution of iron, oxygen and sulphur in the precipitates from C1 (Figures 5C–E) and C5 (Figure 6C–E) indicate a mixture of iron oxide and iron sulphide phases in the precipitates. Notably, a discrete aluminium oxide phase was also detected in the precipitates of both C1 (Fig. S3A–C) and C5 (Fig. S3D–F). It is apparent that aluminium grains lay on top of iron grains, indicating that these have been deposited later during the experiment, as detailed in Fig. S3H–J.

#### *Concentrations of iron in ferrocyanide pond solution post-irradiation*

We measured the concentration of iron in the solutions of *ferrocyanide pond* + *glycine* and *Fe salts-only* experiments with ICP-OES to assess time- and depth-dependent variations. After irradiation of 11 and 14 days, iron concentrations were lowest in the containers strongest exposed to UV (C1–C3), higher in C4 and C5 and remained unchanged from the starting concentration ( $\sim 0.1\text{ mM}$ ) in CD in both experiments (Table 5). The concentration of iron decreased more drastically in the *Fe salts-only* experiment, where the amount of the precipitate was observed to be greater.

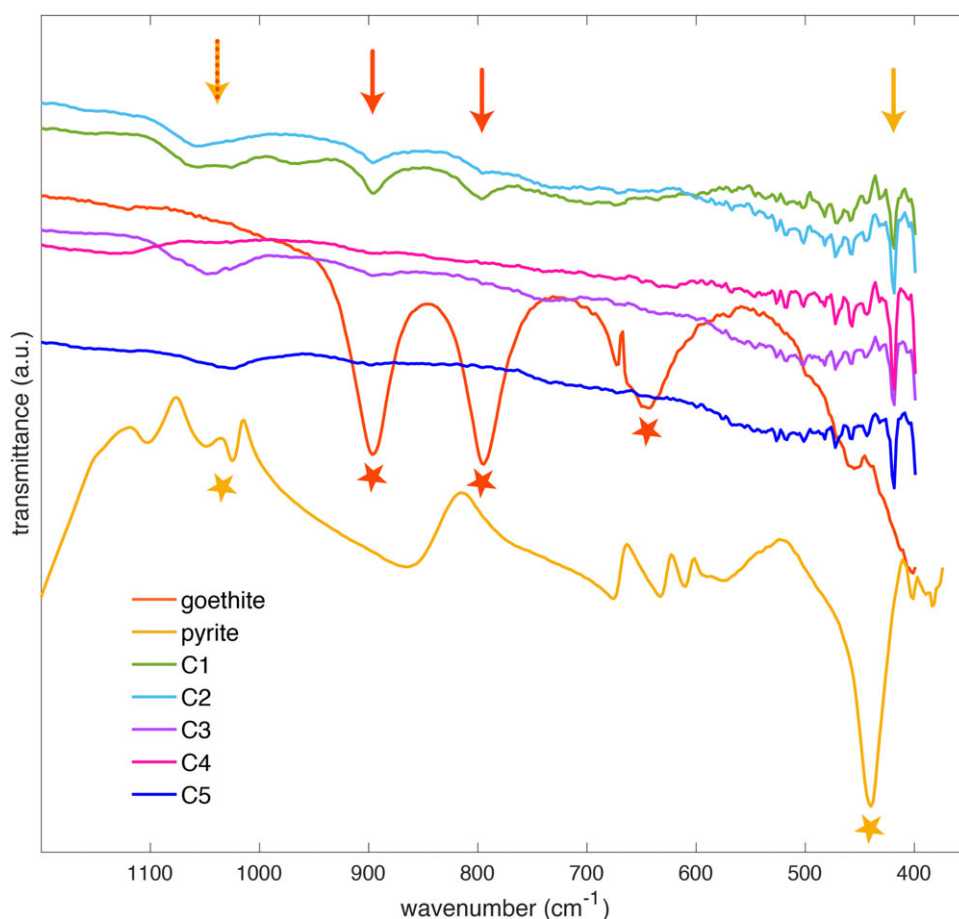


**Figure 4.** Infrared spectrum of the precipitates from containers C1–C5 of the ferrocyanide pond solution after 11 days of irradiation. Pointed out with stars are the prominent peaks in the reference spectra of the minerals goethite and pyrite. The yellow and orange arrows point out the peaks in our precipitates' spectra that may correspond to the peaks of pyrite (yellow) or goethite (orange). The yellow arrow with orange dashes indicates the peak may either correspond to S-S stretching vibration of pyrite, and/or to specifically adsorbed sulphate groups on goethite. The peak values and corresponding vibrational modes are annotated in Table 4.

## UV irradiation of glycine

### Glycine in ultrapure water

Glycine was irradiated in UPW for 6 days and samples were taken at 24-hour intervals. Irradiated glycine in UPW was analysed with nuclear magnetic resonance (NMR) and new chemical shifts in the range of alcohols, ester, ethers, amides and amine-bearing compounds were detected (Figs. S4–S6), suggesting that glycine broke down into diverse photodegradation products during the experiment. The NMR spectra before and after irradiation are shown in Figure 7A. Confirmation of potential photolysis products via spike tests allowed us to identify several, though not all, of the new chemical shifts observed in the NMR spectra, as pointed out in Figure 7A and annotated in Table 6.

The spectrum of glycine after six days of irradiation in C1 served as a basis for new peak detection and is shown against glycine in the same container prior to irradiation in Fig. S7. Reference spectra of all



**Table 4.** Summary of active IR bands corresponding to the peaks marked by stars in the infrared reference spectra of goethite and pyrite (Figure 4) and their vibrational mode assignments.

Band (cm <sup>-1</sup> )	Vibrational mode
1049, 1024	S-S stretching of pyrite
1049, 974	Sulphate groups adsorbed on goethite
895, 799	Fe-O-H bending of goethite
624	Fe-O stretching of goethite
440	Fe-S <sub>2</sub> stretching of pyrite

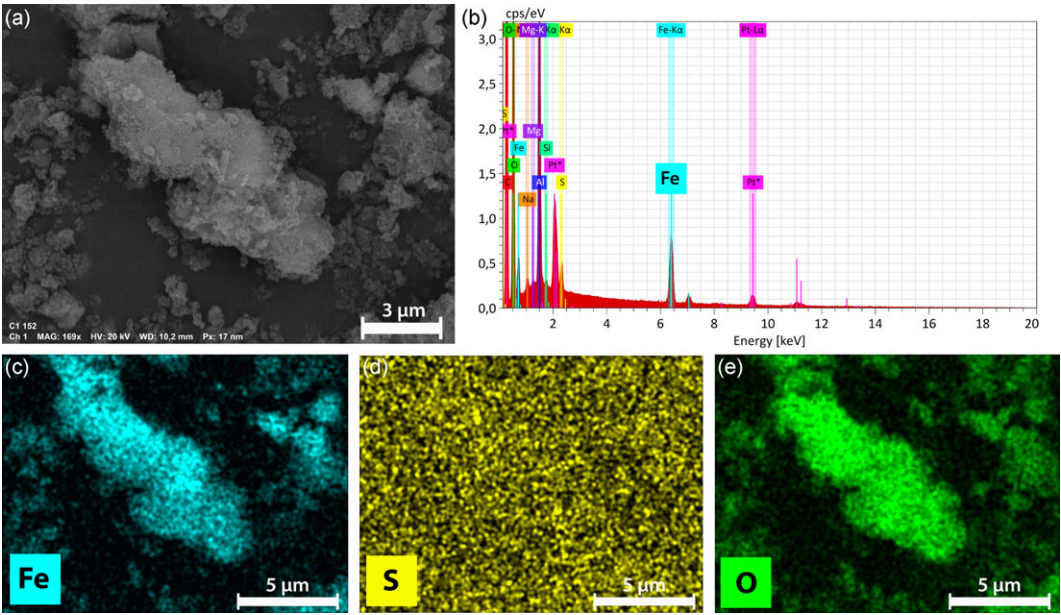


**Figure 5.** (A) Fine-grained precipitate from top container (C1) of ferrocyanide pond solution post irradiation. (B) The EDS spectrum of the precipitate shows amounts of iron, sulphur and oxygen. The distribution of iron (C) and oxygen (E) are uniform in the precipitate, indicating an iron oxide phase. The presence of sulphur also suggests an iron sulphide phase.

potential photodegradation products are shown in Fig. S8. All matching peaks of reference spectra, glycine samples and spiked glycine samples are shown in Fig. S9–15.

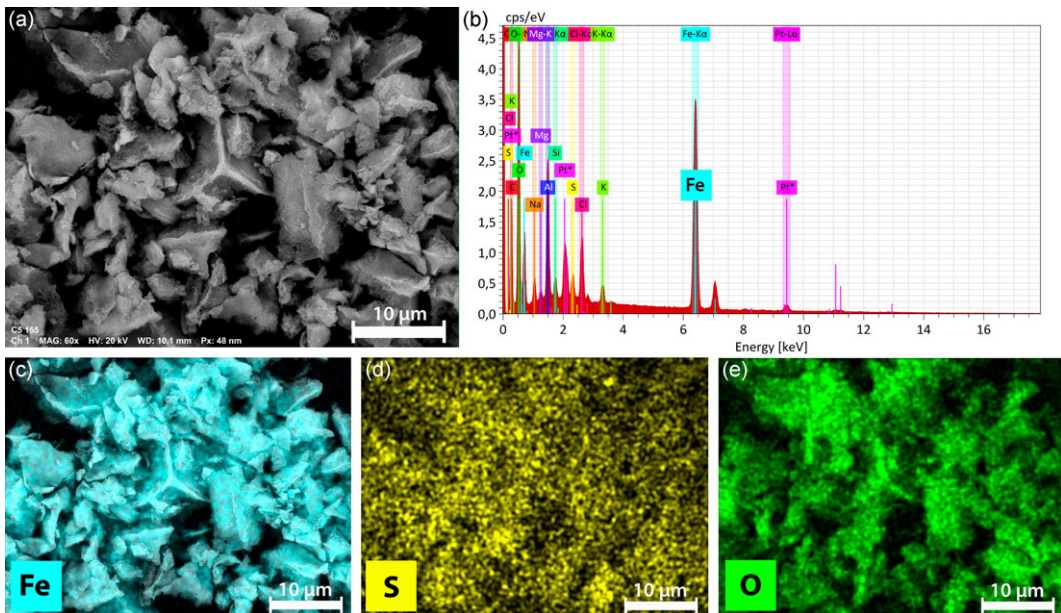
#### *Glycine in ferrocyanide ponds*

Figure 7B shows the degradation products of glycine dissolved in ferrocyanide solutions before and after irradiation for 14 days, with C1 serving as the reference point for detecting new chemical shifts. The degradation products identified include formamide, glycinmethylester, acetaldehyde and ethanol, as detected in the experiment of glycine in UPW (Figure 7A), though glycinamide was not detected.

#### *Glycine in carbonate ponds*

No photodegradation products of glycine were observed in the carbonate solution after irradiation for 14 days (Figure 7C).





**Figure 6.** (A) Crystalline precipitate from bottom container (C5) of ferrocyanide pond solution post irradiation. (B) The EDS spectrum of the precipitate shows amounts of iron, sulphur and oxygen. The distribution of iron (C), sulphur (D) and oxygen (E) are all part of the crystalline structure, indicating a mixture of iron oxide and iron sulphide phases.

## Discussion

### *Comparison of UV protection properties of ferrocyanide and carbonate prebiotic ponds*

Glycine degrades under the influence of UV irradiation (ten Kate *et al.*, 2005; Gerakines *et al.*, 2012; Lee and Kang, 2015). However, the presence of UV-absorbing species could provide significant protection against such radiation (Ranjan *et al.*, 2022; Todd *et al.*, 2022, 2024). To test this hypothesis and add experimental evidence to the subject of prebiotic pond chemistry, we conducted irradiation experiments on glycine in three types of solutions: ultrapure water (UPW), a simulated ferrocyanide prebiotic pond (Table 2) and a saline, carbonate prebiotic pond (Table 3). Our results demonstrate that the UPW solution exhibits great UV transparency, yielding a diverse array of photodegradation products (Figure 7A, Table 6). The ferrocyanide pond also appears to allow for glycine photodegradation (Figure 7B, Table 6) following the formation of a precipitate (Figures 3–6). The carbonate pond offers complete protection against UV-induced degradation, leaving glycine intact throughout the experiment (Figure 7C).

### *UV-induced precipitation and photochemistry in ferrocyanide ponds*

Ferrocyanide ponds may have formed low-UV environments on early Earth due to their high UV-absorbing properties (Ranjan *et al.*, 2022). Our experiments suggest that this effect is only transient as the UV-induced precipitation of ferrocyanide removes it from the solution and in effect clears the water column to allow for the eventual photodegradation of glycine. During irradiation of the ferrocyanide pond, the pH increased from neutral up to ~9 in the solutions. This could be due to the degradation of ferrocyanide through the photoaquation process, which releases free CN<sup>-</sup> that can react with water in solution and increase the concentration of OH<sup>-</sup>, hence increasing pH (Todd *et al.*, 2022). This increase in pH could promote the precipitation of iron oxides and sulphate in the solution.

**Table 5.** Concentrations of iron (mM) identified with ICP-OES for ferrocyanide pond solution with and without glycine prior to and after irradiation. The starting concentration was ~0.1 mM, which remained unchanged in the dark control (CD) in both experiments. All of the iron was precipitated out of the solution in the upper containers after irradiation. The effect was more prominent in the solution without glycine.

Sample	[Fe] (mM)
Ferrocyanide pond solution C1 t11	0.0000
Ferrocyanide pond solution C2 t11	0.0000
Ferrocyanide pond solution C3 t11	0.0020
Ferrocyanide pond solution C4 t11	0.0630
Ferrocyanide pond solution C5 t11	0.0800
Ferrocyanide pond solution CD t11	0.0990
Ferrocyanide pond + glycine C1 t14	0.0000
Ferrocyanide pond + glycine C2 t14	0.0010
Ferrocyanide pond + glycine C3 t14	0.0200
Ferrocyanide pond + glycine C4 t14	0.0670
Ferrocyanide pond + glycine C5 t14	0.0700
Ferrocyanide pond + glycine CD t14	0.0970

After just 1 day of irradiation, the solution in C1–C3 turned yellow and a yellow-orange precipitate was formed in C1 (Figure 3A, B). The container that was not exposed to UV radiation (CD) remained without any discolouration or precipitation, indicating that precipitation is solely triggered by the influence of UV irradiation. The quantity of the precipitate retrieved from the experiment decreased with increasing depth (Figure 3C), though over the course of experiments, it even precipitated out in the lower containers as the upper water column became more UV-transparent (Table S1). Some of the UV could have been blocked from reaching the lower part of the water column by the solid precipitate settling on the Suprasil windows in the upper containers. If so, then it could be expected that in a natural water column without such barriers even more precipitation could be formed as the water becomes increasingly more UV-transparent.

SEM/EDS analysis showed that the precipitate contains iron, oxygen and sulphur in the form of iron oxide, iron sulphide or a mixture of these phases (Figures 5B, C–E and 6B, C–E). In addition, a discrete aluminium oxide phase was seen to be deposited on top of the iron-rich precipitate later during the experiment (Fig. S3). Aluminium was not added as a component to the simulated prebiotic pond solution but was likely leached out from the aluminium-threaded rings of the tower setup over the course of the experiment. The amount of aluminium in the solution was seen to be near the detection limit, indicating it precipitates out immediately after leaching into the solution.

The IR spectra of the precipitate show some resemblance to the spectrum of goethite (iron(III) oxyhydroxide) and pyrite (iron(II) disulphide), exhibiting several peaks that are characteristic of their vibrational modes (Figure 4, Table 4). Goethite reportedly precipitates under the influence of UV radiation in a process called fouling, due to the oxidation-reduction reaction in the presence of radicals (Nessim and Gehr, 2006). With increasing pH  $\text{Fe}^{2+}$  is rapidly oxidized in the presence of radicals, and iron is complexed by hydroxide. This change in chemistry can then cause sulphate to precipitate out and adsorb to the internal and external surfaces of the goethite particles (Musić *et al.*, 2000). Meanwhile, pyrite precipitation is favoured in anoxic, sulphidic environments with slightly alkaline conditions and high dissolved iron and sulphide concentrations, so the presence of both pyrite and goethite is probable in our setup.

We used the dissolution modelling software PHREEQC 3.7.3 (Parkhurst and Appelo, 2013) to understand the potential for goethite and pyrite precipitation in our system and the influence of aluminium concentrations on this process. The MINTEQ database, alongside the sulphite values from the LLNL database, was used as a basis for the model (Wolery, 2013; Allison and Brown, 2015). We

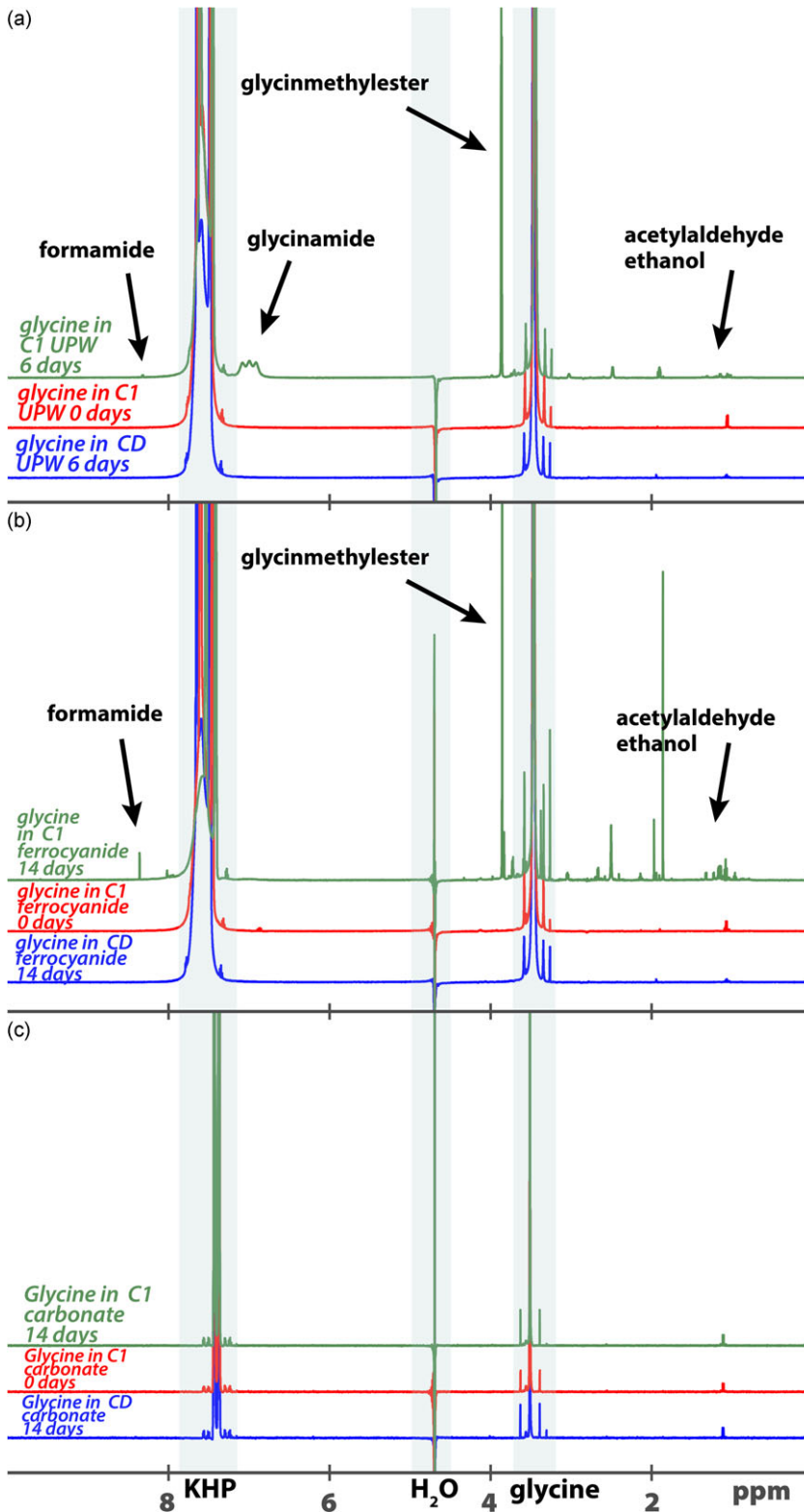


**Table 6.** Summary of NMR results of irradiated glycine in UPW showing new chemical shifts, the proposed range of corresponding products and the corresponding photodegradation products identified by spike tests.

Shift (ppm)	8.33	7.01	3.89	2.51	1.40–1.12
Range	Formic acid, amides	Amides	Alcohols, esters, ethers	Alcohols, amines	Alcohols amines
Identified molecule	Formamide	Glycinamide, formamide	Glycinmethylester	None identified	Acetaldehyde, ethanol

defined an initial solution of 1 L of water at 25°C with a pH of 7.58. An amount of reactant equal to the amount used in the experiments is then irreversibly added to the solution. The newly created solution represents the experimental solution without the presence of aluminium. In order to study the influence of aluminium, 50 simulations were run adding between 0 and 1 mmol of aluminium in steps of 0.02 mmol. The resulting pH levels and saturation indices for goethite, pyrite and aluminium oxide can be seen in Figure 8. The addition of aluminium decreased the pH from ~10.5 with no aluminium to ~8.8 with 1.0 mM aluminium. If more than 0.7 mM aluminium was present in the solution, the saturation index for goethite was below zero, meaning goethite would most likely not precipitate. However, if less than 0.6 mM aluminium was present, the saturation index for goethite was positive; therefore, goethite could have precipitated. The saturation index of pyrite was positive regardless of aluminium content and could thus always precipitate. This is in accordance with our FTIR and SEM/EDS data, where we initially observed the precipitation of goethite in C1 and C2 (Figures 4, 5 and S1), while pyrite precipitation proceeded throughout the experiment in containers C1–C5 (Figures 4, 6 and S2).

According to our experimental results and simulations, we propose the following chemical chain of events in our ferrocyanide pond experiment:

1. Ferrocyanide is broken down by UV through the photoaquation process (Equation 5), increasing the pH of the solution.
2. The increase in pH results in the precipitation of goethite and pyrite, removing iron from the solution.
3. This increase in pH also causes aluminium to begin leaching out of the tower rings.
4. As aluminium leaches into the system, the pH of the solution decreases, halting goethite precipitation.
5. As the iron is removed from the solution, aluminium hydroxide is deposited over the iron-rich precipitate.

In a realistic ferrocyanide pond without any aluminium, we could thus still expect the UV-induced precipitation of both goethite and pyrite minerals. The amount of precipitate formed in the *ferrocyanide pond* + glycine experiment was less than in the *Fe salts-only* experiment, in accordance with the amount

**Figure 7.** <sup>1</sup>H NMR spectra of glycine solutions in simulated prebiotic ponds before and after UV irradiation. Highlighted in light blue are the residual water signal at 4.70 ppm, the internal standard (KHP) shifts at 7.66 and 7.51 ppm and the glycine shift at 3.5 ppm. Sidebands due to the natural abundance of <sup>13</sup>C are visible for KHP and glycine. (?) Glycine in UPW before (red) and after (green) irradiation and dark control (blue). After 6 days, five regions of the spectrum show new peaks identified with spike tests as formamide (8.33 ppm), glycinamide (7.01 ppm), glycinmethylester (3.89 ppm) and acetaldehyde/ethanol (1.40–1.12 ppm). (B) Glycine in ferrocyanide pond before and after irradiation. After 14 days glycine degraded into formamide, glycinmethylester and acetaldehyde/ethanol. (C) Glycine in carbonate pond before and after irradiation. After 14 days, no UV-induced changes occurred in the spectrum.

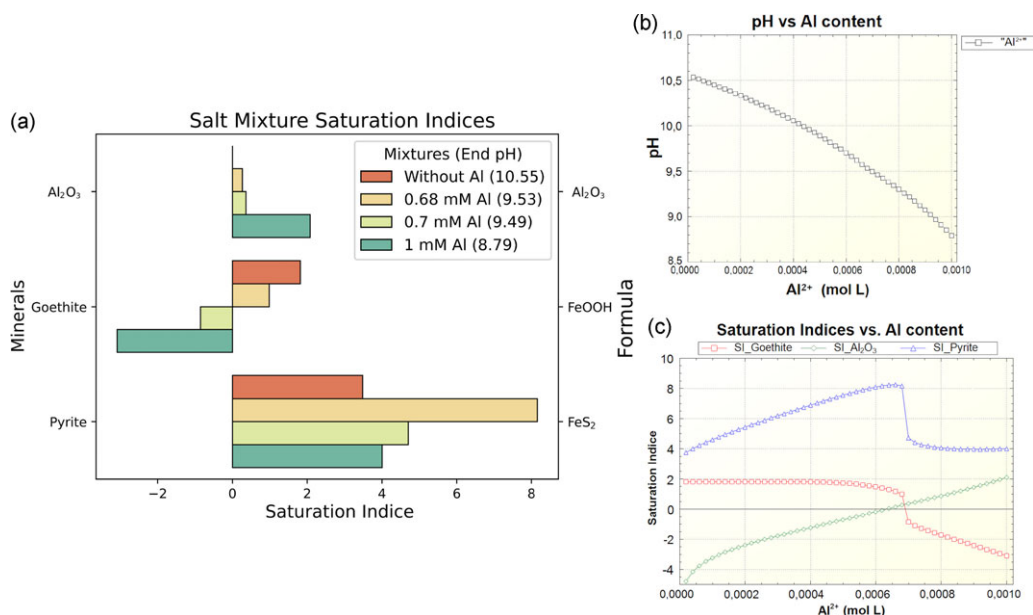


**Figure 8.** PHREEQC modelling results show the potential for goethite and pyrite precipitation in the ferrocyanide pond solution. (A) Goethite is precipitated when there is no Al in the system. Pyrite precipitates at all explored concentrations of Al. Aluminium oxide precipitates at higher concentrations of Al. (B) The addition of  $\text{Al}^{2+}$  into the system lowers the initial pH. (C) The addition of aluminium into the system inhibits the precipitation goethite and partially influences the formation of pyrite.

of iron left in the solution (Table 5). Glycine appears to have stabilized the particles in our solution and reduced the rate of aggregation of iron. The presence of naturally dissolved organic matter, in our case glycine, can indeed stabilize nanoparticles in water and reduce their rate of aggregation by imparting a negative charge to the surface and increasing the absolute surface potential of nanoparticles. The adsorption of natural organic matter can increase the electric double-layer repulsive energy and enhance a net energy barrier between nanoparticles. This can lead to stabilization and less aggregation of nanoparticles in water (Zhang *et al.*, 2009).

Since organic carbon cannot be discriminated with our SEM/EDS setup, we could not elucidate whether glycine was adsorbing to the precipitate particles or if it was in any way contributing to the precipitate formation. Glycine adsorbed onto particles could potentially settle together with the precipitate and thus be preserved in the sediments or lower water levels. Moreover, mineral surfaces are known to catalyse prebiotic chemistry and can also drive polymerization (Kitadai *et al.*, 2017), which might be crucial for origin-of-life chemistry in ferrocyanide ponds. Though the specifics of the mineral- and radical-induced chemistry in this setup are not possible to measure, it is apparent that following the precipitation of ferrocyanide, glycine degrades into a variety of photoproducts (Figure 7B), be it from direct photolysis (Equations 1 and 2) or from interaction with residual ferrocyanide radicals (Equations 4 and 5).

Thus, the ferrocyanide pond presents us with a transiently protective and chemically dynamic environment, with ferrocyanide shielding the glycine from UV radiation until it is precipitated out (Figure 9). After the UV processing of a ferrocyanide pond, we can expect to find goethite and pyrite mineral assemblages in the paleolake sedimentary record.

#### UV protection and resulting stability in carbonate ponds

In saline, carbonate ponds,  $\text{Br}^-$  is the strongest absorber followed by  $\text{NO}_3^-$  and  $\text{Cl}^-$ , all of which have high absorption coefficients, particularly at short wavelengths (Ranjan *et al.*, 2022). Our results suggest



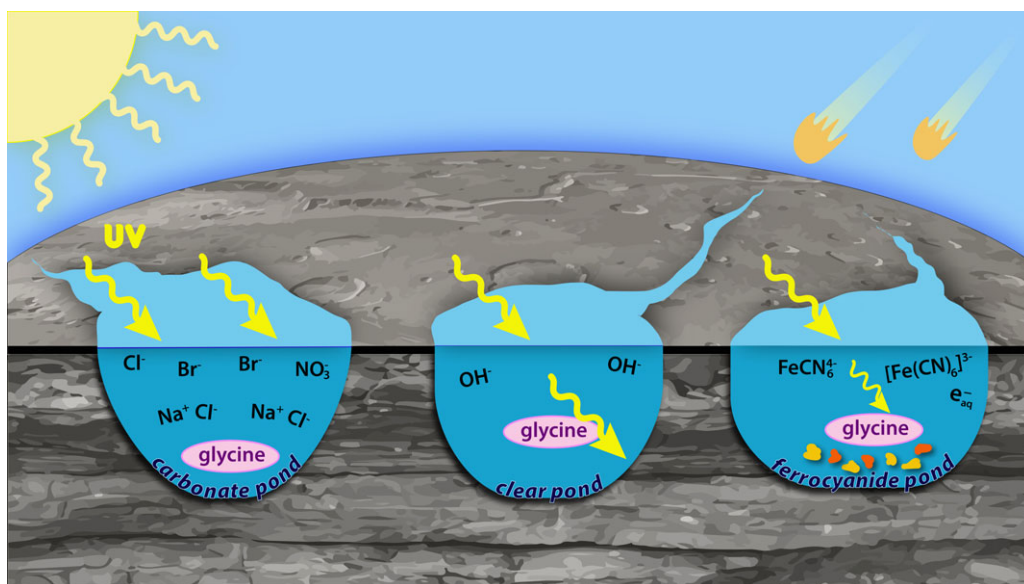


**Figure 9.** Dissolved ions may have served as “sunscreens” molecules in the aqueous solutions of shallow prebiotic ponds, thus enhancing preservation organic molecules delivered by meteorites. In a clear pond, nothing protects glycine from photodegradation. A ferrocyanide pond offers a transiently protective environment and will deposit goethite and pyrite mineral assemblages in the paleolake sedimentary record. In a carbonate pond, UV radiation is strongly absorbed by ions such as Br<sup>−</sup> and Cl<sup>−</sup> and glycine is protected by a “salting-in” effect due to high concentrations of NaCl.

that hypersaline, carbonate ponds may present a stable environment under UV radiation for glycine by providing a constant strong UV attenuation since no photodegradation products were detected after 14 days of irradiation (Figure 7C). This suggests that no radicals or high-energy species were produced by UV-absorbing compounds during our experiments, though this has been described to occur in the literature (Jortner, 1964; Sauer *et al.*, 2004). Instead, the glycine is protected from photodegradation by UV-absorbing anions and not subjected to further radical chemistry. Our findings suggest that saline, carbonate solutions could provide great stability and UV-shielding for amino acids. Whether carbonate ponds would provide the same stability for other organic molecules such as nucleobases cannot be extrapolated from these results, as nucleobases absorb at longer UV wavelengths.

In the presence of very high concentrations of salts (here 3 M NaCl), amino acid properties such as solubility, denaturation or thermodynamic activity can be affected. While high salt concentration generally causes amino acids to precipitate out of solution due to a “salting-out effect,” experiments have shown that in the Gly-NaCl-H<sub>2</sub>O system, the activity of glycine decreases with increasing NaCl concentrations, giving rise to a “salting-in” effect for amino acids (Sirbu and Iulian, 2010). The ions in the solution can shield glycine from the charge of other amino acids present in the solution, for example. This effect results in enhanced solubility and stability of glycine. Our results suggest that high salt concentrations could produce such a salting-in effect in saline, carbonate ponds, as shown in the schematic in Figure 9.

### **Implications for astrobiology**

The concept of prebiotic ponds as potential sites for the origin of life was first proposed by Charles Darwin in 1871. In this study, we investigated two promising types of such ponds: ferrocyanide ponds and carbonate ponds. Both are found on many rocky bodies in our solar system and offer intriguing avenues in the search for habitable environments in space exploration.



*Transient ferrocyanide ponds on Mars offer a window into prebiotic Earth*

Ferrocyanide ponds are extensively investigated within the field of prebiotic chemistry, as HCN serves as a fundamental precursor for the synthesis of amino acids and nucleotides. Furthermore, the combination of ferrocyanide with sulphite can engage in UV-induced photoredox cycles, facilitating the generation of solvated electrons. These electrons play a critical role in the reduction of cyanide, leading to the formation of essential biomolecular compounds including sugars and amino acid, nucleotide and lipid precursors (Todd *et al.*, 2022). The stability and formation of ferrocyanide are influenced by environmental conditions: optimal formation rates and yields occur under slightly alkaline conditions (pH 8–9) and moderate temperatures (approximately 20–30°C). As showcased in this work and others, ferrocyanide is susceptible to degradation under near-UV light (300–400 nm) (Todd *et al.*, 2024).

Prebiotic chemistry is thought to have occurred in aqueous environments on a warm and wet Noachian Mars (Brack, 2018; Schulze-Makuch *et al.*, 2008). The Martian geological record can in turn inform us about the geochemical conditions of prebiotic Earth, where this record is largely lacking. While they may have been rare on early Earth, transient ferrocyanide lakes have been proposed as prebiotic venues on early Mars (Sasselov *et al.*, 2020). In such lakes, ferrocyanide would have been delivered periodically by meteorite impacts and later precipitated into the sedimentary record in episodic drying events, presenting a transiently protective and dynamical chemical environment. The setup we have built has allowed us to experimentally study this complex planetary geochemical process. Our results from the ferrocyanide pond experiments suggest that goethite and pyrite mineral assemblages would be expected in the sedimentary records of ferrocyanide paleolakes on Mars. The laboratory spectra of these minerals obtained here will be useful as reference spectra to compare to measurements taken by Curiosity in Gale Crater and by Perseverance in Jezero Crater. We would encourage the targeting of these mineral assemblages by Perseverance for the Mars Sample Return (MSR) campaign.

*Brines across the Solar System present a multitude of potential cradles for life*

Saline, carbonate aqueous solutions, often referred to as brines, are widely distributed across multiple celestial bodies within our solar system. On Mars, geological evidence indicates the existence of saline lakes in the past, with extensive evaporite deposits suggesting the presence of magnesium sulphate-rich brines on early Mars (Vaniman *et al.*, 2004; Olsen *et al.*, 2015; Fox-Powell *et al.*, 2016). Observations of Ceres, the only dwarf planet in the inner Solar System, suggest the presence of subsurface brines that could maintain a liquid water ocean beneath its surface, raising intriguing possibilities about its geological activity and potential habitability (Daswani and Castillo-Rogez, 2022). Meanwhile, Jupiter's moon Europa and Saturn's moon Enceladus are believed to possess subsurface oceans containing saline water. The detection of sodium carbonates and halite in plumes and surface deposits supports the existence of alkaline brines within these moons (Postberg *et al.*, 2009; Trumbo *et al.*, 2019). Recent analyses of samples from asteroids Ryugu and Bennu have revealed the presence of sodium carbonates and other evaporite minerals, indicating that these bodies once harboured highly saline, alkaline brines. The detection of such minerals suggests that these asteroids underwent processes involving liquid water, which subsequently evaporated or froze, leaving behind salt deposits (Matsumoto *et al.*, 2024; McCoy *et al.*, 2025).

Furthermore, carbonate ponds present viable solutions to several persistent challenges in origin-of-life research. Notably, they address the “phosphate problem” which arises from the low bioavailability of phosphate in natural waters, typically insufficient for the synthesis of essential biomolecules. In these environments, calcium preferentially precipitates as carbonate minerals rather than forming insoluble apatite through binding with phosphate. Thus, the accumulation of phosphate in these ponds would facilitate many prebiotic syntheses (Toner and Catling, 2020). Intertwined, the “nitrogen problem” concerns the availability of bioavailable nitrogen compounds required for amino acid and nucleotide synthesis. Studies of modern soda lakes, such as Last Chance Lake in Canada, reveal that high salinity can suppress nitrogen fixation rates, allowing for significant phosphate accumulation, which favours

prebiotic chemical processes (Haas *et al.*, 2024). Lastly, as demonstrated in this study and by (Ranjan *et al.*, 2022), high-salinity, carbonate waters create a protective environment against harmful UV radiation. This property supports the stability and longevity of prebiotic molecules, enhancing the plausibility of these settings as cradles for life's emergence.

These findings highlight the potential of carbonate ponds to address these key challenges, establishing them as promising environments for prebiotic chemical processes. Hence, studying brines across diverse planetary bodies advances our understanding of aqueous environments in the Solar System and offers significant insights into planetary processes and potential habitats for life.

## Conclusion

Prebiotic waters may have contained UV-absorbing compounds that functioned as protective agents, shielding organic molecules in solution from UV-induced photodegradation. We built a modular, multicompartment tower to study the UV-driven photochemistry of organic molecules in shallow ponds with diverse geochemical parameters and the suitability of those ponds for prebiotic chemistry in origin-of-life studies. With this setup, we performed irradiation experiments wherein glycine was exposed to UV light in ultrapure water and in simulated prebiotic pond environments rich in ferrocyanide and carbonate. Assuming the simulated solar spectra used in this study are realistic for early Earth surface illumination up to 400 nm, the processes occurring in our setup are indicative of the UV-induced organic chemistry taking place in hypothetical early Earth environments. Further work would include the incorporation of different geochemical parameters and other organic species into our solutions to study (in)organic chemistry of diverse aqueous venues.

Our study provides valuable insights into the behaviour of glycine in aqueous solutions representative of ferrocyanide and carbonate prebiotic ponds. Our findings indicate that glycine's photochemical degradation under UV irradiation is minimal in the carbonate pond, but significant in the ferrocyanide pond and the pure water pond (Figure 9). Ferrocyanide is recognized as a potent UV absorber, however, the UV-induced processes that eventually generated precipitate containing goethite and pyrite during our ferrocyanide pond experiments contributed to its removal, thereby exposing glycine to UV degradation. This implies that ferrocyanide ponds could be transiently good places for prebiotic chemistry (e.g. in transient ponds on Mars in the aftermath of large impacts). The targeting of goethite and pyrite mineral assemblages in Martian paleolake sediments by the MSR campaign could provide further insight into these processes on early Earth. On the other hand, the carbonate ponds provided a UV-stable environment in our setup by protecting glycine from photodegradation and radical chemistry. Considering the benefits of saline ponds (their ability to preserve phosphate in bioavailable forms for example) and the widespread presence of brines throughout the Solar System, these environments could serve as reservoirs of organic carbon molecules, ensuring their preservation and stability in the prebiotic conditions of early Earth and other celestial bodies.

**Supplementary material.** The supplementary material for this article can be found at <https://doi.org/10.1017/S1473550425100098>.

**Acknowledgements.** We express gratitude to the GeoLab (Utrecht University) members for their support in the upkeep of the laboratories. We express a special recognition to Mariette Wolthers who guided us with PHREEQC simulations. We thank the anonymous reviewer for their poignant and thoughtful feedback with which we were able to improve the manuscript.

**Funding statement.** The work of A.Z. was supported by the Dutch Research Council (NWO) grant PEPSci-19.007. The work of N.K. was supported by the NWO grant ALWOP.274. The work of L.J. and S.L.L. was supported by the Olaf Schuiling Fund. The work of H.v.I. was supported by the uNMR-NL Grid: A distributed, state-of-the-art Magnetic Resonance facility for the Netherlands (NWO grant 184.035.002).

**Competing interests.** The author(s) declare none.

## References

- Allison JD and Brown DS (2015) MINTEQA2/PRODEFA2—a geochemical speciation model and interactive preprocessor. In *Chemical Equilibrium and Reaction Models*, pp. 241–252. <https://doi.org/10.2136/SSASPECPUB42.C12>
- Bada JL and Korenaga J (2018) Exposed areas above sea level on earth >3.5 Gyr ago: implications for prebiotic and primitive biotic chemistry. *Life* **8**, 55. <https://doi.org/10.3390/LIFE8040055>
- Bahcall JN, Pinsonneault MH and Basu S (2001) Solar models: current epoch and time dependences, neutrinos, and helioseismological properties. *The Astrophysical Journal* **555**, 990–1012. <https://doi.org/10.1086/321493/XML>
- Birkmann J, Pasel C, Luckas M and Bathen D (2018) UV spectroscopic properties of principal inorganic ionic species in natural waters. *Water Practice and Technology* **13**, 879–892. <https://doi.org/10.2166/WPT.2018.097>
- Brack A (2018) An origin of life on Mars? In *From Habitability to Life on Mars*, pp. 13–35. <https://doi.org/10.1016/B978-0-12-809935-3.00001-3>
- Cambier P (1986) Infrared study of goethites of varying crystallinity and particle size: I. Interpretation of OH and lattice vibration frequencies. *Clay Minerals* **21**, 191–200. <https://doi.org/10.1180/CLAYMIN.1986.021.2.08>
- Camprubi E, de Leeuw JW, House CH, Raulin F, Russell MJ, Spang A, Tirumalai MR and Westall F (2019) The emergence of life. *Space Science Reviews*. <https://doi.org/10.1007/s11214-019-0624-8>
- Chyba C and Sagan C (1992) Endogenous production, exogenous delivery and impact-shock synthesis of organic molecules: an inventory for the origins of life. *Nature* **355**, 125–132. <https://doi.org/10.1038/355125A0>
- Claire MW, Sheets J, Cohen M, Ribas I, Meadows VS and Catling DC (2012) The evolution of solar flux from 0.1 nm to 160  $\mu$ m: quantitative estimates for planetary studies. *Astrophysical Journal* **757**. <https://doi.org/10.1088/0004-637X/757/1/95>
- Cnossen I, Sanz-Forcada J, Favata F, Witasse O, Zegers T and Arnold NF (2007) Habitat of early life: solar X-ray and UV radiation at Earth's surface 4–3.5 billion years ago. *Journal of Geophysical Research: Planets* **112**, EO2008-doi: [10.1029/2006JE002784](https://doi.org/10.1029/2006JE002784). <https://doi.org/10.1029/2006JE002784>
- Cobb AK and Pudritz RE (2014) Nature's starships. I. observed abundances and relative frequencies of amino acids in meteorites. *Astrophysical Journal* **783**. <https://doi.org/10.1088/0004-637X/783/2/140>
- Cockell CS (2000) The ultraviolet history of the terrestrial planets — implications for biological evolution. *Planetary and Space Science* **48**, 203–214. [https://doi.org/10.1016/S0032-0633\(99\)00087-2](https://doi.org/10.1016/S0032-0633(99)00087-2)
- Cruz-Cruz LP, Negrón-Mendoza A and Heredia-Barbero A (2020) Stability of glycine in saline solutions exposed to ionizing radiation. *Journal of Nuclear Physics, Material Sciences, Radiation and Applications* **7**, 83–87. <https://doi.org/10.15415/JNP.2020.72009>
- Damer B and Deamer D (2020) The hot spring hypothesis for an origin of life. *Astrobiology*. <https://doi.org/10.1089/ast.2019.2045>
- Daswani MM and Castillo-Rogez JC (2022) Porosity-filling metamorphic brines explain ceres's low mantle density. *Planetary Science Journal* **3**, 21. <https://doi.org/10.3847/PSJ/AC4509>
- de Jager TL, Cockrell AE and Du Plessis SS (2017) Ultraviolet light induced generation of reactive oxygen species. *Advances in Experimental Medicine and Biology* **996**, 15–23. [https://doi.org/10.1007/978-3-319-56017-5\\_2](https://doi.org/10.1007/978-3-319-56017-5_2)
- Deamer D and Weber AL (2010) Bioenergetics and life's origins. *Cold Spring Harbor Perspectives in Biology* **2**, a004929. <https://doi.org/10.1101/CSHPERSPECT.A004929>
- Djokic T, Van Kranendonk MJ, Campbell KA, Havig JR, Walter MR and Guido DM (2021) A reconstructed subaerial hot spring field in the ~3.5 billion-year-old dresser formation, North Pole Dome, Pilbara Craton, Western Australia. <https://home.liebertpub.com/ast> **21**, 1–38. <https://doi.org/10.1089/AST.2019.2072>
- Ehrenfreund P, Bernstein MP, Dworkin JP, Sandford SA and Allamandola LJ (2001) The photostability of amino acids in space. *The Astrophysical Journal* **550**, L95–L99. <https://doi.org/10.1086/319491>
- Fernández-García C, Coggins AJ and Powner MW (2017) A chemist's perspective on the role of phosphorus at the origins of life. *Life* **7**, 31. <https://doi.org/10.3390/LIFE7030031>
- Fornaro T, Boosman A, Brucato JR, ten Kate IL, Siljeström S, Poggiali G, Steele A and Hazen RM (2018) UV irradiation of biomarkers adsorbed on minerals under Martian-like conditions: Hints for life detection on Mars. *Icarus* **313**, 38–60. <https://doi.org/10.1016/J.ICARUS.2018.05.001>
- Fox S, Pleyer HL and Strasdeit H (2019) An automated apparatus for the simulation of prebiotic wet-dry cycles under strictly anaerobic conditions. *International Journal of Astrobiology* **18**, 60–72. <https://doi.org/10.1017/S1473550418000010>
- Fox SW and Harada K (1958) Thermal copolymerization of amino acids to a product resembling protein. *Science* **128**, 1214. <https://doi.org/10.1126/SCIENCE.128.3333.1214>
- Fox-Powell MG, Hallsworth JE, Cousins CR and Cockell CS (2016) ionic strength is a barrier to the habitability of Mars. *Astrobiology* **16**, 427–442. <https://doi.org/10.1089/AST.2015.1432>
- Garry JRC, Loes ten Kate I, Martins Z, Nørnberg P and Ehrenfreund P (2006) Analysis and survival of amino acids in Martian regolith analogs. *Meteoritics and Planetary Science* **41**, 391–405. <https://doi.org/10.1111/J.1945-5100.2006.TB00470.X>
- Gerakines PA, Hudson RL, Moore MH and Bell JL (2012) In situ measurements of the radiation stability of amino acids at 15–140K. *Icarus* **220**, 647–659. <https://doi.org/10.1016/J.ICARUS.2012.06.001>
- Glavin DP, Conel CMO, Aponte JC, Dworkin JP, Elsila JE and Yabuta H (2018) The origin and evolution of organic matter in carbonaceous chondrites and links to their parent bodies. In *Primitive Meteorites and Asteroids: Physical, Chemical, and Spectroscopic Observations Paving the Way to Exploration*, pp. 205–271. <https://doi.org/10.1016/B978-0-12-813325-5.00003-3>
- Gotić M and Musić S (2007) Mössbauer, FT-IR and FE SEM investigation of iron oxides precipitated from FeSO<sub>4</sub> solutions. *Journal of Molecular Structure* **834–836**, 445–453. <https://doi.org/10.1016/J.MOLSTRUC.2006.10.059>

- Gough DO (1981) Solar interior structure and luminosity variations. *Solar Physics* **74**, 21–34. <https://doi.org/10.1007/BF00151270/METRICS>
- Haas S, Sinclair KP and Catling DC (2024) Biogeochemical explanations for the world's most phosphate-rich lake, an origin-of-life analog. *Communications Earth & Environment* **5**(1), 1–11. <https://doi.org/10.1038/s43247-023-01192-8>
- Han G, Wen S, Wang H and Feng Q (2020) Interaction mechanism of tannic acid with pyrite surfaces and its response to flotation separation of chalcopyrite from pyrite in a low-alkaline medium. *Journal of Materials Research and Technology* **9**, 4421–4430. <https://doi.org/10.1016/J.JMRT.2020.02.067>
- Johnson PV, Hodyss R, Chernow VF, Lipscomb DM and Goguen JD (2012) Ultraviolet photolysis of amino acids on the surface of icy Solar System bodies. *Icarus* **221**, 800–805. <https://doi.org/10.1016/J.ICARUS.2012.09.005>
- Jortner J (1964) On the photochemistry of aqueous solutions of chloride, bromide, and iodide ions. *Journal of Physical Chemistry* **68**, 247–255. [https://doi.org/10.1021/J100784A005/ASSET/J100784A005.FP.PNG\\_V03](https://doi.org/10.1021/J100784A005/ASSET/J100784A005.FP.PNG_V03)
- Kitadai N, Oonishi H, Umemoto K, Usui T, Fukushi K and Nakashima S (2017) Glycine polymerization on oxide minerals. *Origins of Life and Evolution of Biospheres* **47**, 123–143. <https://doi.org/10.1007/S11084-016-9516-Z/FIGURES/8>
- Lafuente B, Downs RT, Yang H and Stone N (2016) The power of databases: the RRUFF project. In *Highlights in Mineralogical Crystallography*, pp. 1–29. <https://doi.org/10.1515/9783110417104-003>
- Lahav N, White D and Chang S (1978) Peptide formation in the prebiotic era: thermal condensation of glycine in fluctuating clay environments. *Science* (1979) **201**, 67–69. <https://doi.org/10.1126/SCIENCE.663639>
- Lee CW and Kang H (2015) UV photolysis of glycine on ice films: implication for photosynthesis and photodestruction of amino acids in interstellar medium#. *Bulletin of the Korean Chemical Society* **36**, 784–788. <https://doi.org/10.1002/BKCS.10145>
- Maciá E (2005) The role of phosphorus in chemical evolution. *Chemical Society Reviews* **34**, 691–701. <https://doi.org/10.1039/B416855K>
- Matsumoto T, Noguchi T, Miyake A, Igami Y, Matsumoto M, Yada T, Uesugi M, Yasutake M, Uesugi K, Takeuchi A, Yuzawa H, Ohigashi T and Araki T (2024) Sodium carbonates on Ryugu as evidence of highly saline water in the outer Solar System. *Nature Astronomy* **8**, 1536–1543. <https://doi.org/10.1038/s41550-024-02418-1>
- McCoy TJ, Russell SS, Zega TJ, Thomas-Keprta KL, Singerling SA, Brenker FE, Timms NE, Rickard WDA, Barnes JJ, Libourel G, Ray S, Corrigan CM, Haenecour P, Gainsforth Z, Dominguez G, King AJ, Keller LP, Thompson MS, Sandford SA, Jones RH, Yurimoto H, Righter K, Eckley SA, Bland PA, Marcus MA, DellaGiustina DN, Ireland TR, Almeida NV, Harrison CS, Bates HC, Schofield PF, Seifert LB, Sakamoto N, Kawasaki N, Jourdan F, Reddy SM, Saxey DW, Ong IJ, Prince BS, Ishimaru K, Smith LR, Benner MC, Kerrison NA, Portail M, Guigoz V, Zanetta P-M, Wardell LR, Gooding T, Rose TR, Salge T, Le L, Tu VM, Zesut Z, Mayers C, Sun X, Hill DH, Lunning NG, Hamilton VE, Glavin DP, Dworkin JP, Kaplan HH, Franchi IA, Tait KT, Tachibana S, Connolly HC and Lauretta DS, 2025. An evaporite sequence from ancient brine recorded in Bennu samples. *Nature* **637**, 1072–1077. <https://doi.org/10.1038/s41586-024-08495-6>
- Melton CE and Neece GA (1971) Rate constants and cross sections for the production of OH- from O- and H- in water. *Journal of the American Chemical Society* **93**, 6757–6759. <https://doi.org/10.1021/JA00754A007>
- Musić S, Šarić A, Popović S, Nomura K and Sawada T (2000) Forced Hydrolysis of Fe<sup>3+</sup> Ions in NH<sub>4</sub>Fe(SO<sub>4</sub>)<sub>2</sub> Solutions Containing Urotropin. *Croatica Chemica Acta* **73**, 541–567.
- Nessim Y and Gehr R (2006) fouling mechanisms in a laboratory-scale UV disinfection system. *Water Environment Research* **78**, 2311–2323. <https://doi.org/10.2175/106143006X95474>
- Olsen AA, Hausrath EM and Rimstidt JD (2015) Forsterite dissolution rates in Mg-sulfate-rich Mars-analog brines and implications of the aqueous history of Mars. *Journal of Geophysical Research* **120**, 388–400. <https://doi.org/10.1002/2014JE004664>
- Oró J and Holzer G (1979) The photolytic degradation and oxidation of organic compounds under simulated Martian conditions. *Journal of Molecular Evolution* **14**, 153–160. <https://doi.org/10.1007/BF01732374>
- Osinski GR, Cockell CS, Pontefract A and Sapers HM (2020) The role of meteorite impacts in the origin of life. *Astrobiology* **20**, 1121–1149. [https://doi.org/10.1089/AST.2019.2203/ASSET/IMAGES/LARGE/AST.2019.2203\\_FIGURE8.JPEG](https://doi.org/10.1089/AST.2019.2203/ASSET/IMAGES/LARGE/AST.2019.2203_FIGURE8.JPEG)
- Pace NR (1991) Origin of life—facing up to the physical setting. *Cell* **65**, 531–533. [https://doi.org/10.1016/0092-8674\(91\)90082-A](https://doi.org/10.1016/0092-8674(91)90082-A)
- Parkhurst DL and Appelo CAJ (2013) Description of Input and Examples for PHREEQC Version 3—A Computer Program for Speciation, Batch-Reaction, One-Dimensional Transport, and Inverse Geochemical Calculations. US geological survey techniques and methods 497.
- Patel BH, Percivalle C, Ritson DJ, Duffy CD and Sutherland JD (2015) Common origins of RNA, protein and lipid precursors in a cyanosulfidic protometabolism. *Nature Chemistry* **7**, 301–307. <https://doi.org/10.1038/NCHEM.2202>
- Pearce BKD, Molaverdikhani K, Pudritz RE, Henning T and Cerrillo KE (2022) Toward RNA life on early earth: from atmospheric HCN to biomolecule production in warm little ponds. *The Astrophysical Journal* **932**, 9. <https://doi.org/10.3847/1538-4357/AC47A1>
- Poch O, Noblet A, Stalport F, Correia JJ, Grand N, Szopa C and Coll P (2013) Chemical evolution of organic molecules under Mars-like UV radiation conditions simulated in the laboratory with the “Mars organic molecule irradiation and evolution” (MOMIE) setup. *Planetary and Space Science* **85**, 188–197. <https://doi.org/10.1016/J.PSS.2013.06.013>
- Postberg F, Kempf S, Schmidt J, Brilliantov N, Beinsen A, Abel B, Buck U and Srama R (2009) Sodium salts in E-ring ice grains from an ocean below the surface of Enceladus. *Nature* **459**, 1098–1101. <https://doi.org/10.1038/nature08046>
- Ranjana S, Kufner CL, Lozano GG, Todd ZR, Haseki A and Sasselov DD (2022) UV transmission in natural waters on prebiotic earth. *Astrobiology* **22**, 242–262. <https://doi.org/10.1089/ast.2020.2422>



- Ricardo A, Carrigan MA, Olcott AN and Benner SA (2004) Borate minerals stabilize ribose. *Science* **303**, 196. <https://doi.org/10.1126/SCIENCE.1092464>
- Rossetto D, Valer L, Martín NY, Guella G, Hongo Y and Mansy SS (2022) Prebiotic environments with Mg<sup>2+</sup> and thiophilic metal ions increase the thermal stability of cysteine and non-cysteine peptides. *ACS Earth and Space Chemistry* **6**, 1221–1226. [https://doi.org/10.1021/ACSEARTHSPACECHEM.2C00042/ASSET/IMAGES/LARGE/SP2C00042\\_0003.JPEG](https://doi.org/10.1021/ACSEARTHSPACECHEM.2C00042/ASSET/IMAGES/LARGE/SP2C00042_0003.JPEG)
- Santosh M, Arai T and Maruyama S (2017) Hadean Earth and primordial continents: the cradle of prebiotic life. *Geoscience Frontiers* **8**, 309–327. <https://doi.org/10.1016/J.GSF.2016.07.005>
- Sasselov DD, Grotzinger JP and Sutherland JD (2020) The origin of life as a planetary phenomenon. *Science Advances* **6**. <https://doi.org/10.1126/SCIADV.AAX3419/ASSET/508DF664-BF45-4ACE-9C94-6E0CE9A1EA50/ASSETS/GRAPHIC/AAX3419-F4.JPEG>
- Sauer MC, Crowell RA and Shkrob IA (2004) Electron photodetachment from aqueous anions. 1. Quantum yields for generation of hydrated electron by 193 and 248 nm laser photoexcitation of miscellaneous inorganic anions. *Journal of Physical Chemistry A* **108**, 5490–5502. [https://doi.org/10.1021/JP049722T/SUPPL\\_FILE/JP049722TSI20040420\\_113554.PDF](https://doi.org/10.1021/JP049722T/SUPPL_FILE/JP049722TSI20040420_113554.PDF)
- Schulze-Makuch D, Fairén AG and Davila AF (2008) The case for life on Mars. *International Journal of Astrobiology* **7**, 117–141. <https://doi.org/10.1017/S1473550408004175>
- Schwartz AW (2006) Phosphorus in prebiotic chemistry. *Philosophical Transactions of the Royal Society B: Biological Sciences* **361**, 1743–1749. <https://doi.org/10.1098/RSTB.2006.1901>
- Sephton MA (2014) Organic geochemistry of meteorites. In *Treatise on Geochemistry: Second Edition*. <https://doi.org/10.1016/B978-0-08-095975-7.01002-0>
- Sirbu F and Iulian O (2010) The mixing effect of glycine with sodium chloride from activity coefficients investigations at T = (303.15 and 313.15) K. *Journal of Optoelectronics and Advanced Materials* **12**, 1200–1205.
- Stetter KO (2005) Volcanoes, hydrothermal venting, and the origin of life. In *Volcanoes and the Environment*, pp. 175–206. <https://doi.org/10.1017/CBO9780511614767.007>
- ten Kate IL, Garry JRC, Peeters Z, Foing B and Ehrenfreund P (2006) The effects of Martian near surface conditions on the photochemistry of amino acids. *Planetary and Space Science* **54**, 296–302. <https://doi.org/10.1016/J.PSS.2005.12.002>
- ten Kate IL, Garry JRC, Peeters Z, Quinn R, Foing B and Ehrenfreund P (2005) Amino acid photostability on the Martian surface. *Meteoritics & Planetary Science* **40**, 1185–1193. <https://doi.org/10.1111/J.1945-5100.2005.TB00183.X>
- ten Kate IL and Reuver M (2016) PALLAS: planetary analogues laboratory for light, atmosphere, and surface simulations. *Netherlands Journal of Geosciences* **95**, 183–189. <https://doi.org/10.1017/NJG.2015.19>
- Tian F, Kasting JF and Zahnle K (2011) Revisiting HCN formation in Earth's early atmosphere. *E&PSL* **308**, 417–423. <https://doi.org/10.1016/J.EPSL.2011.06.011>
- Todd ZR, Lozano GG, Kufner CL, Ranjan S, Catling DC and Sasselov DD (2024) UV transmission in prebiotic environments on early earth. *Astrobiology* **24**, 559–569. [https://doi.org/10.1089/AST.2023.0077/ASSET/IMAGES/AST.2023.0077\\_FIGURE6.JPG](https://doi.org/10.1089/AST.2023.0077/ASSET/IMAGES/AST.2023.0077_FIGURE6.JPG)
- Todd ZR, Lozano GG, Kufner CL, Sasselov DD and Catling DC (2022) Ferrocyanide survival under near ultraviolet (300–400 nm) irradiation on early Earth. *Geochimica et Cosmochimica Acta* **335**, 1–10. <https://doi.org/10.1016/J.GCA.2022.08.012>
- Toner JD and Catling DC (2020) A carbonate-rich lake solution to the phosphate problem of the origin of life. *Proceedings of the National Academy of Sciences of the United States of America* **117**, 883–888. [https://doi.org/10.1073/PNAS.1916109117/SUPPL\\_FILE/PNAS.1916109117.SAPP.PDF](https://doi.org/10.1073/PNAS.1916109117/SUPPL_FILE/PNAS.1916109117.SAPP.PDF)
- Toner JD and Catling DC (2019) Alkaline lake settings for concentrated prebiotic cyanide and the origin of life. *Geochimica et Cosmochimica Acta* **260**, 124–132. <https://doi.org/10.1016/J.GCA.2019.06.031>
- Trumbo SK, Brown ME and Hand KP (2019) Sodium chloride on the surface of Europa. *Science Advances* **5**, 7123–7135. [https://doi.org/10.1126/SCIADV.AAW7123/SUPPL\\_FILE/AAW7123\\_SM.PDF](https://doi.org/10.1126/SCIADV.AAW7123/SUPPL_FILE/AAW7123_SM.PDF)
- van Kranendonk MJ (2010) Two types of Archean continental crust: plume and plate tectonics on early earth. *American Journal of Science* **310**, 1187–1209. <https://doi.org/10.2475/10.2010.01>
- Vaniman DT, Bish DL, Chipera SJ, Fialips CI, Carey JW and Feldman WG (2004) Magnesium sulphate salts and the history of water on Mars. *Nature* **431**, 663–665. <https://doi.org/10.1038/NATURE02973>
- Verdonck L, Hoste S, Roelandt FF and Van Der Kelen GP (1982) Normal coordinate analysis of  $\alpha$ -FeOOH - a molecular approach. *Journal of Molecular Structure* **79**, 273–279. [https://doi.org/10.1016/0022-2860\(82\)85065-5](https://doi.org/10.1016/0022-2860(82)85065-5)
- Watt GD, Christensen JJ and Izatt RM (1965) thermodynamics of metal cyanide coordination. III.  $\Delta G^\circ$ ,  $\Delta H^\circ$ , and  $\Delta S^\circ$  values for ferrocyanide and ferricyanide ion formation in aqueous solution at 25°. *Inorganic Chemistry* **4**, 220–222. [https://doi.org/10.1021/IC50027A026/ASSET/IC50027A026.FP.PNG\\_V03](https://doi.org/10.1021/IC50027A026/ASSET/IC50027A026.FP.PNG_V03)
- Westheimer FH (1987) Why nature chose phosphates. *Science* **235**, 1173–1178. <https://doi.org/10.1126/SCIENCE.2434996>
- Wogan NF, Catling DC, Zahnle KJ and Lupu R (2023) Origin-of-life molecules in the atmosphere after big impacts on the early earth. *Planetary Science Journal* **4**, 169. <https://doi.org/10.3847/PSJ/ACED83>
- Wolery TJ (2013) EQ3/6 - Software for Geochemical Modeling, Version 8.0a, LLNL-CODE-2013-683958 [WWW Document]. Lawrence Livermore National Laboratory, Livermore, CA. [https://github.com/LLNL/EQ3\\_6](https://github.com/LLNL/EQ3_6) (accessed 2.20.25).
- Xu J, Ritson DJ, Ranjan S, Todd ZR, Sasselov DD and Sutherland JD (2018) Photochemical reductive homology of hydrogen cyanide using sulfite and ferrocyanide. *Chemical Communications* **54**, 5566–5569. <https://doi.org/10.1039/C8CC01499J>
- Yoshida T, Koyama S, Nakamura Y, Terada N and Kuramoto K (2024) self-shielding enhanced organics synthesis in an early reduced earth's atmosphere. *Astrobiology* **24**, 1074–1084. [https://doi.org/10.1089/AST.2024.0048/ASSET/IMAGES/AST.2024.0048\\_FIGURE12.JPG](https://doi.org/10.1089/AST.2024.0048/ASSET/IMAGES/AST.2024.0048_FIGURE12.JPG)

- Zahnle KJ (1986) Photochemistry of methane and the formation of hydrocyanic acid (HCN) in the Earth's early atmosphere. *Journal of Geophysical Research: Atmospheres* **91**, 2819–2834. <https://doi.org/10.1029/JD091ID02P02819>
- Zahnle KJ, Lupu R, Catling DC and Wogan N (2020) Creation and evolution of impact-generated reduced atmospheres of early earth. *Planetary Science Journal* **1**, 11. <https://doi.org/10.3847/PSJ/AB7E2C>
- Zetterlind AO, Potisil C, Sanders TJ, Hoefnagels B, van der Tak FFS and ten Kate IL (2024) Insights into the liberation of organic matter and the aqueous alteration of carbonaceous chondrites exposed to prebiotic ponds. In LPICo, vol. 3036, p. 6378.
- Zhang Y, Chen Y, Westerhoff P and Crittenden J (2009) Impact of natural organic matter and divalent cations on the stability of aqueous nanoparticles. *Water Research* **43**, 4249–4257. <https://doi.org/10.1016/J.WATRES.2009.06.005>
- Zheng K, Li H, Xu L, Li S, Wang L, Wen X and Liu Q (2019) The influence of humic acids on the weathering of pyrite: electrochemical mechanism and environmental implications. *Environmental Pollution* **251**, 738–745. <https://doi.org/10.1016/J.ENVPOL.2019.05.060>